

Referee #1:

5 *One thing not addressed in the paper is the relationship between the number of views and their diversity. It is not the number of views that matter but their diversity. It should be noted that views that have similar geometry and polarization do not really add to the measurement diversity, and so do not add information to the wind retrieval process. Such measurements can be grouped (averaged) into a “super” view that is treated as a single view without affecting the wind retrieval. In fact, this is frequently done when processing rotating pencil-beam scatterometers: sigma-0 measurements with similar views (“flavors” in the QuikSCAT literature) are often averaged to simply processing. For this paper there must be a way to*
10 *quantify the diversity of the views (other than just using their number). This should be used to investigate how the diversity contributes the FOMs’ value. Bottom line: adding additional views that do not have distinctly different geometry (i.e., that do not really add to the diversity) cannot be expected to improve the wind retrieval. Such additional measurements are essentially only improving the effective SNR of the class (super view) of similar views rather than adding new geometric information need to improve the wind retrieval.*

15

An experiment has been done to verify the influence of the views with similar geometry. The following text has been added in discussion session:

20 One question is raised here: is the azimuth diversity the major influencer in the wind retrieval quality or the number of views with similar azimuth also give added value in the wind retrieval process? The views with similar azimuth geometry are averaged together into one super view. This influences most of the nadir swath since the views are with mainly forward and backward azimuths. Figure 23 shows that the views with similar azimuth angle in one of the nadir WVCs are aggregated into one view and the views for the nadir swath becomes mainly one forward and one backward. The wind retrieval results (Figure 24) in comparison with the normal wind retrieval results (Figure 17) show that the wind retrieval result with all the
25 WVCs looks very similar, which seems that the views with similar azimuth angle do not have much added value onto the wind retrieval process, but when the outer swath WVCs are excluded from the result, wind speed and wind direction (Figure 24 (b)) are both worse than Figure 17 (b) as well as when excluding the nadir swath. In Figure 17 (b) and (c), the nadir swath does not influence the wind speed retrieval much, while here (Figure 24 (b) and (c)) the wind speed and wind direction retrieval results are obviously improved after excluding nadir swath. This means the reduction of the number of views in the
30 nadir swath after aggregating the views with similar azimuth angle into one view leads to a worse wind retrieval quality.

Referee #2:

Page 3, Line 3: Question: Have either SCAT or WindRad been launched? Are there any references to their design and on-orbit performance?
5

SCAT has been launched on 29th Oct 2018, but WindRad has not been launched yet and the plan is this year. The reference of SCAT design and on-orbit performance is at session 2.1 'The RFSCAT characteristics have been studied and assessed by Lin et al. (Lin et al., 2000a, 2002)'. The reference for WindRad is added in the manuscript:

10 The scatterometer (referred to as SCAT from now on) onboard CFOSAT (China-France Oceanography SATellite) and WindRad (Chinese Wind Radar on FY-3E) belong to this type of scatterometer and are planned to be launched in 2018 and 2019 (Dou et al., 2014).

15 Page 5, Tables 1, 2, and 3

Correction: What is currently listed as "antenna bandwidth" in the table is perhaps more appropriately termed "center frequency."

Yes, it has been corrected (see table 1, 2, and 3).

20

Recommendation: In Tables 1-3 include the actual TRANSMIT BANDWIDTH in the table. This would be extremely valuable for the readers to understand how many independent range looks are available for each slice measurement. (For instance, from the literature SeaWinds has a transmit bandwidth of 375 kHz.).

25 They are added in Tables 1-3.

Recommendation: Specifically state the number of independent looks (not views) for each slice.

30 The technical parameters are not able to get for CFOSAT and WindRad (they are not allowed to release to public from the China part). The simulation does not use the number of independent looks for each slice, we simplified the simulation by cutting slices the same size from the pulse, so unfortunately, we do not have the number of independent looks for each slice.

Recommendation: In Tables 1-3 add what the Noise Equivalent sigma-0 is for each system. Perhaps it is actually a range of values depending on the specific slice position within the antenna footprint on the ground.

5 It is indeed a range of values depending on the specific slice position within the antenna footprint. The NESZ plots for all the antennas of each scatterometer are added in the manuscript after the Tables 1-3.

Text are added in 2.1:

10 NESZ (Noise Equivalent Sigma-Zero) is a range of values depending on the specific slice position within the antenna footprint on the ground. Figure 3, Figure 4, and Figure 5 give the NESZ distribution as a function of the slice number for SCAT, WindRad and SeaWinds.

Recommendation: Add a new diagram/figure showing how each antenna footprint is "sliced" using range processing. What are the dimensions of the individual slices on the ground? What is the overall spatial resolution of each system?

15 In the simulation, the slicing is simplified by cutting the pulse into the equal length slices, so maybe it is not necessary to have a diagram, and text is added in session 2.3 'In order to simplify the simulation procedure, the pulse is cut into equal size slices.'

20 It is two dimensions of the individual slices on the ground. The overall spatial resolutions are CFOSAT 10km, WindRad (C-band 20km, Ku-band 10km), SeaWinds 25km.

Page 7, Lines 1-5: Comment: The authors are correct in indicating that the coefficients A, B, and C are a function of the precise detection scheme. The approximations for A, B, and C given in the paper are identical to those derived for SeaWinds, which uses a deramp detection of the chirped bandwidth and then frequency filtering to obtain each slice. It is unclear whether they are applicable to the SCAT or WindRad cases because the detection scheme is not specified.

Question: I don't understand what the statement "The distribution of Bs on each slice in one pulse is assigned according to the antenna gain pattern of the pulse" means.

30 We do not have the access to the detection scheme of CFOSAT and WindRad, so the approximation is applied here. The approximation is to give distribute the pulse bandwidth onto slices with the distribution pattern of antenna gain pattern. The antenna gain pattern has the feature that peak at the center and gradually decreasing to the sides as a function of the distance to the center. So, the slice_bandwidth = pulse_bandwidth * antenna_pattern.

Page 9, Figure 6: Question: What are you defining as being a "view." Specifically, for SeaWinds, my understanding is that for the outer WVC's, there are measurements that occur from multiple azimuth angles for multiple antenna rotation, although it is a very small range of azimuth angle variation). For instance, in the paper "Point-Wise Wind Retrieval and Ambiguity Removal Improvements for the QuikSCAT Climatological Data Set," A.G. Fore et. al., IEEE Trans. on Geosci. and Remote Sensing, VOL 52, No. 1, January 2014, it shows a distinct "saddle shaped" distribution of "composites" as a function of WVC, not a flat distribution as shown in the author's Figure 6. What is the difference between "composites" in the above paper and "views" in this paper?

10 For SeaWinds, the classic way of defining the views is that the slices in one WVC are classified by fore/after beam first and then within the inner swath, the slices are classified by their polarization into two views (VV and HH), so there are four views at the inner swath. The outer swath only has one polarization, so it only has two views (fore/after beams). The definition of the composites in the paper (2014) is not very clear, they used a new method to aggregate the slices into one WVC, but the next step of grouping into views is not clearly described, so I would think the definition of composites is different from the views in my paper.

Page 10, Lines 4,5: Comment: The line that reads "... the Kpc on the WVC level is derived by averaging the Kpc for all the views in the corresponding WVC." Wouldn't the Kpc instead be actually reduced when all the views of included together? As multiple s_0 's from different views are averaged, wouldn't the aggregate Kpc go down?

20 Yes, the Kpc will go down with the averaging all views or slices together and to reduce Kpc is important as well.

Pages 14 and 15: Question: Figures 10 and 11 appear to be a model simulation output whereas Figure 12 is an actual SeaWinds measured wind field (?).

They are all simulated output. The purpose of these figures is to show that 2DVAR has been working in the simulation, so where to select the area is not important.

30 Page 20, Line 20: Comment: The statement "Overall the wind retrieval performance of the rotating fan-beam instruments is better than the pencil-beam instrument." Clearly more "views" are better than fewer views, but the number of looks is also important. This conclusion may be the case for this specific pencil-beam scatterometer (SeaWinds) with its relatively small bandwidth and low number of looks per slice, but a pencil beam scatterometer with a higher gain and/or higher transmit bandwidth could potentially compensate for the lack of views. There may be a trade-off here.

Yes, this trade-off is possible. In general, the number of views and the geometry diversity of the views play a major part in the wind retrieval quality, and the higher transmit bandwidth will lead to a high number of looks per slice thus leads to a better retrieval result. The number of views of rotating fan beam is significantly larger than pencil beam, so this trade-off might play a less important role here.

Page 25, Conclusions: Comment: One aspect that I find seriously missing in this paper is the acknowledgement that SeaWinds (as well as SCAT and WindRad maybe?) have already been operating in orbit. In the case of SeaWinds, there is an approximately 10-year data record that has been extensively evaluated. Yet the actual performance of the scatterometers on actual wind fields is not compared to the model simulation results. It seems that this would be a good means of establishing the validity of the model, particularly with regards to evaluating the “geophysical noise.” The chances are good, I would guess, that the model performance is actually better than that observed in the real world in all cases. Thus the model/simulation evaluation might best be said to be an evaluation of “relative performance potential” amongst various scatterometer designs as opposed to actual real world performance.

The SCAT is in the orbit now (still in calibration process, not ready for release), and WindRad is not launched yet. The validation between simulated SeaWinds and actual SeaWinds data is a good evaluation for the simulation system and it has been done now, the following texts are added:

‘2.4.1 Simulation model validation

SeaWinds is chosen as the validation data in comparison with simulated data since it has worked about 10 years and the other two scatterometers do not have sufficient data. All the scatterometers’ simulation orbit is the same as CFOSAT in order to have a good inter-comparison among the three scatterometers and it is different from the actual orbit of SeaWinds, so there are in total 77866 collocated WVCs (one day 14 orbits data) and Figure 9 shows the collocated wind retrieval result. The simulated wind speed and wind direction give a good correlation to the real SeaWinds data, which means the simulation model has good performance, and it is suitable for the comparison among the different type of scatterometers.’

A Generalized Simulation Capability for Rotating Beam Scatterometers

Moved down [1]: A Generalized Simulation Capability for Rotating Beam Scatterometers

Moved (insertion) [1]

Zhen Li¹, Ad Stoffelen¹, Anton Verhoef¹

¹R&D Satellite Observation, Royal Netherlands Meteorological Institute, de Bilt, 3731 GA, Netherlands

Correspondence to: Zhen Li (li@knmi.nl)

Abstract. Rotating-beam wind scatterometers exist in two types: rotating fan-beam and rotating pencil-beam. In our study, a generic simulation frame is established and verified to assess the wind retrieval skill of the three different scatterometers: SCAT on CFOSAT, WindRad on FY-3E and SeaWinds on QuikScat. Besides the comparison of the so-called 1st rank-resolution retrieval skill of the input wind field, other Figure of Merits (FoMs) are applied to statistically characterize the associated wind retrieval performance from three aspects: wind vector root mean square error, ambiguity susceptibility, and wind biases. The evaluation shows that, overall, the wind retrieval quality of the three instruments can be ranked from high to low as WindRad, SCAT, and SeaWinds, where the wind retrieval quality strongly depends on the Wind Vector Cell (WVC) location across the swath. Usually, the higher the number of views, the better the wind retrieval, but the effect of increasing the number of views reaches saturation, considering the fact that the wind retrieval quality at the nadir and sweet swath parts stays relatively similar for SCAT and WindRad. On the other hand, the wind retrieval performance in the outer swath of WindRad is improved substantially as compared to SCAT due to the increased number of views. The results may be generally explained by the different incidence angle ranges of SCAT and WindRad, mainly affecting azimuth diversity around nadir and number of views in the outer swath. This simulation frame can be used for optimizing the Bayesian wind retrieval algorithm, in particular to avoid biases around nadir, but also to investigate resolution and accuracy through incorporating and analysing the spatial response functions of the simulated Level-1B data for each WVC.

1 Introduction

The wind scatterometer has been proven to be a powerful instrument for global sea surface wind measurement. The wind retrievals have a wide variety of applications, including now-casting, and assimilation in numerical weather prediction models, as well as oceanography, climate research, and off-shore energy applications (Offiler, 1984; Naderi et al., 1991; Stoffelen and Anderson, 1997; Portabella, 2002; Bajo et al., 2017). The wind retrieval is achieved by inverting a set of radar cross-section measurements (σ^0) at different geometries (incidence and/or azimuth look angles) over a Wind Vector Cell

(WVC) through a Geophysical Model Function (GMF) to extract the wind. The more diversity in the geometry, the better wind retrieval will be achieved (Portabella, 2002).

Currently, there are two types of scatterometer in orbit: multiple fixed fan-beam and rotating pencil-beam instruments.

The first wind scatterometer in space was the SEASAT-A Scatterometer System (SASS) on SEASAT-A launched in June

5 1978 by NASA with four fixed fan beams and dual co-polarization (VV and HH) Ku-band (13.2 GHz) emitting and receiving antennas, which failed in October 1978 (Offiler, 1984). The term 'views' in this paper means measurements of the surface σ^0 at different azimuth angle and/or incidence angle and/or polarizations, and each surface σ^0 measurement is aggregated from the samples with the same polarization, similar azimuth and incidence angle. The geometric diversity of the views is able to improve the wind retrieval accuracy. 'Views' is different from the term 'looks' in radar which is defined as

10 the equivalent number of independent samples in a particular σ^0 measurement and specifies the measurement variance (Ulaby and Long, 2013). This scatterometer had two views only per Wind Vector Cell (WVC), a VV view and an HH view, which turned out insufficient to well resolve the wind direction unambiguously. The ERS-1 and -2 satellites carried a scatterometer onboard as of 1991 three fixed fan beams and vertical co-polarization (VV) at C-band frequency (5.4 GHz), with all beams pointing to the right-hand side of the satellite. After ERS-1/2, the NASA Scatterometer (NSCAT) was
15 launched in 1996 on the Japanese Advanced Earth Observing Satellite (ADEOS-I). It had six fan beams with VV capability on the fore and after beams, and both VV and horizontal (HH) co-polarization on the mid beams (Naderi et al., 1991). The European Space Agency (ESA) developed the Advanced Scatterometer (ASCAT) on the Metop satellite series, which has six C-band VV fan beams, each 3 pointing to the left and right of the swath resp., and it started to provide data in 2006 (Gelsthorpe et al., 2000). The ERS-1/2, NSCAT and ASCAT instruments all use three independent views per WVC, leading
20 to a reduced wind direction ambiguity as compared to SASS, by well sampling the main second harmonic wind direction dependency of the Geophysical Model Function (GMF) (Stoffelen and Anderson, 1997; Stoffelen and Portabella, 2006).

SeaWinds, the first rotating pencil-beam scatterometer was developed by NASA and launched on QuikSCAT (1999), on the Japanese satellite ADEOS-2 (2003) and flew as RapidScat on the International Space Station in 2014. It has two Ku-band rotating pencil-beams measuring VV and HH, respectively, at two fixed incidence angles (Hoffman and Leidner, 2005). All

25 current and prior rotating pencil-beam scatterometers are similar in design concept to SeaWinds and differ primarily in the used incidence angles. The OSCAT scatterometer on Oceansat-2 is a Ku-band rotating pencil-beam instrument similar to SeaWinds and developed by the Indian Space Research Organization (ISRO). It was launched in 2009 and failed in 2014 (Singh et al., 2012). After that, ISRO launched SCATSat-1 in 2016 as an OceanSat-2 replacement mission with the same scatterometer design and OceanScat-3 will be launched in 2018. China launched its first Ku-band rotating pencil-beam
30 scatterometer on board HY-2A in 2011 and operating until present (Jiang et al., 2012). SeaWinds-class rotating pencil-beam scatterometers are able to obtain four independent views per WVC in the inner swath, but only two independent views per WVC in the outer swath, where only vertically polarized views are available. This will impose similar ambiguity problems as in the SASS design.

Deleted: and

Formatted: Font: Times New Roman, 10 pt, Font color: Auto, English (UK), Snap to grid, Pattern: Clear

Formatted: Font: Times New Roman, 10 pt, Font color: Auto, English (UK), Snap to grid, Pattern: Clear

Formatted: Font: Times New Roman, 10 pt, Font color: Auto, English (UK), Snap to grid, Pattern: Clear

Deleted: This type of

Deleted: is

A new type of scatterometer – the Rotating Fan-beam Scatterometer (RFSCAT) in Ku-band was proposed in 2000 (Lin et al., 2000b). It combines the features from fixed fan-beam and rotating pencil-beam scatterometers, which provide large swath coverage and increase the diversity in the observation geometry. The scatterometer (referred to as SCAT from now on) onboard CFOSAT (China-France Oceanography SATellite) and WindRad (Chinese Wind Radar on FY-3E) belong to this type of scatterometer and are planned to be launched in 2018 and 2019 (Dou et al., 2014). These represent a rotating fan-beam instrument with Ku-band only (SCAT), a rotating fan-beam instrument with both Ku and C-band (WindRad), and a rotating pencil-beam instrument with Ku-band only (SeaWinds).

The aim of our study is to build a generic simulation system and construct an evaluation frame, particularly fit for the above rotating-beam scatterometers, including Ku-band and C-band. The simulation system includes the complete simulation of satellite orbital movement, Level-1B (L1B) data generation, Level-2A (L2A) data generation and Level-2B (L2B) wind retrieval. The three different rotating-beam scatterometers are expected to perform differently, due to their varying observation geometry and non-linear wind retrieval characteristics, e.g., wind direction ambiguity. The wind retrieval results are carefully evaluated and compared. The advantages and disadvantages are analyzed such that they can be used as design reference.

2 Simulation method

2.1 CFOSAT, WindRad and SeaWinds characteristics

The RFSCAT characteristics have been studied and assessed by Lin et al. (Lin et al., 2000a, 2002). The slowly rotating fan-beam sweeps over the swath and the different views overlap in each WVC, which leads to multiple views in a given WVC (Figure 1). Contrary to the fixed fan-beam and rotating pencil-beam instruments, the number of views in a WVC depends on its location and varies across the swath as a function of the rotating speed. The scanning geometry results in a smaller number of views and less azimuth diversity in the outer and the nadir parts of the swath, which lead to a degraded wind retrieval performance. In contrast, the other region of the swath (named as sweet swath) has a better wind retrieval performance than the outer and nadir swath.

SCAT and WindRad are both rotating fan-beam designs, but they have somewhat different characteristics. They both follow the RFSCAT principles, but SCAT has two fan beams operating in Ku-band with VV and HH respectively, whereas WindRad has four fan beams. Two of these beams are operating in Ku-band at VV and HH respectively while the other two are operating VV or HH in C-band. All the antennas transmit and receive pulses in turns (see the illustrations in Figure 1). The main parameters for simulating SCAT and WindRad are listed in Table 1 and Table 2.

Rotating pencil-beam scatterometers have been flying on several satellites as described in the Introduction. SeaWinds is taken as representative for the rotating pencil-beam design in our study. It has one dish antenna of about 1 m diameter with a VV and HH beam conically scanning at a speed of 18 rpm, which is much faster than the rotating fan-beam (Figure 2). The

Deleted: Figure 1

Formatted: Font: Times New Roman, Font color: Auto, English (UK), Snap to grid

Deleted: Table 1

Deleted: Table 2

Formatted: Font: Times New Roman, Font color: Auto, English (UK), Snap to grid

Formatted: Font: Times New Roman, Font color: Auto, English (UK), Snap to grid

Deleted: Figure 2

VV beam has a higher incidence angle than the HH beam, resulting in a wider VV swath. There are four integrated views produced at all WVCs; for those located in the inner swath by segregating both VV and HH and fore and aft views. The four views in the outer swath that are used in the retrieval are all VV views, also divided into resp. fore and aft views, but each split in two azimuth groups. The main parameters of the SeaWinds instrument are listed in [Table 3](#).

NESZ (Noise Equivalent Sigma-Zero) is a range of values depending on the specific slice position within the antenna footprint on the ground. Figure 3, Figure 4, and Figure 5 give the NESZ distribution as a function of the slice number for SCAT, WindRad and SeaWinds.

- Deleted:** Table 3
- Formatted:** Font: (Default) +Body (Times New Roman)
- Formatted:** Font: Not Italic, Font color: Auto, English (UK), Snap to grid
- Formatted:** Font: Not Italic, Font color: Auto, English (UK), Snap to grid
- Formatted:** Font: Not Italic, Font color: Auto, English (UK), Snap to grid
- Formatted:** Font: Times New Roman, Font color: Auto, English (UK), Snap to grid
- Formatted:** Font: Times New Roman, Font color: Auto, English (UK), Snap to grid
- Formatted:** Font: Times New Roman, Font color: Auto, English (UK), Snap to grid
- Deleted:** ¶
- Formatted:** Font: (Default) Times New Roman

5
10
15
20
25
30
35

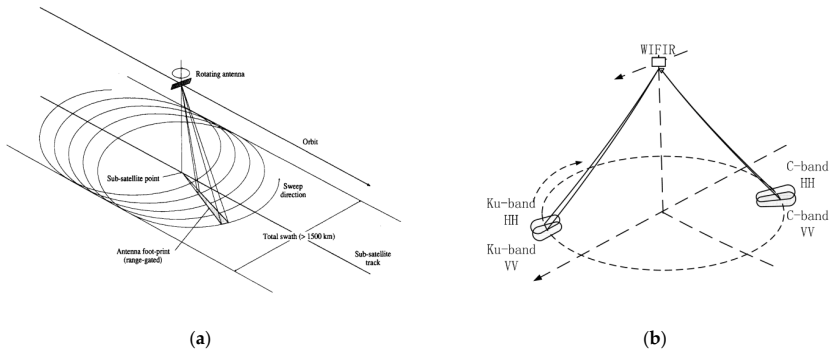


Figure 1: Rotating fan-beam scatterometer. (a) SCAT (Lin et al., 2000a); (b) WindRad (Dou et al., 2014).

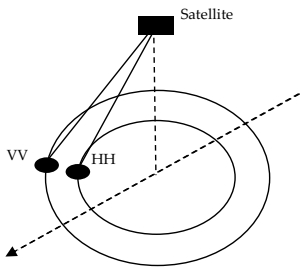


Figure 2: Rotating pencil-beam scatterometer.

Table 1. Main parameters of CFOSAT SCAT

Parameters	Value
Orbit height	514 km
Swath	1000 km
Footprint	280 km
Satellite speed	7.1 km/s
Antenna rotating speed	3.5 rpm
Polarization	VV and HH alternating
Incidence angle range	25 – 48 deg
Antenna pointing angle	40 deg
Peak transmit power	120 W
WVC resolution	25 km
Center frequency	13.256 GHz (Ku-band)
Duration of transmit pulse	1.3 ms
Duration of receiving pulse	2.7 ms
Pulse Repetition Frequency (PRF)	75 Hz
Two-way -3dB beam width (azimuth)	1.28 deg
Peak antenna gain	30 dB
Transmit bandwidth	0.5 MHz

Table 2. Main parameters of FY-3E WindRad

Parameters	Value	
	Ku-band	C-band
Orbit height		836 km
Swath		1400 km
Footprint		200 km
Satellite speed		7.4 km/s
Antenna rotating speed		3.0 rpm
Polarization		VV and HH alternating
Incidence angle range		34.7 – 44.5 deg
Antenna pointing angle		34.8 deg
WVC resolution		25 km
Peak transmit power	120 W	100 W
Center frequency	13.256 GHz	5.4 GHz
Duration of transmit pulse	1.8 ms	1.7 ms
Duration of receiving pulse	1.25 ms	1 ms
Pulse Repetition Frequency (PRF)	208 Hz	104 Hz
Two-way -3dB azimuth beam width	1.3 deg	0.52 deg
Peak antenna gain	37 dB	32 dB
Transmit bandwidth		0.6 MHz

Deleted: ¶

Deleted: ¶
¶
¶
¶

Deleted: Antenna bandwidth

Deleted: Antenna bandwidth

Formatted: Centered

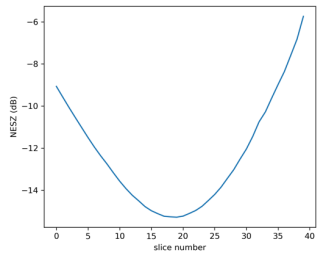
Table 3. Main parameters of QuikScat SeaWinds

Parameters	Value (inner and outer beam)
Orbit height	800 km
Swath	1800 km
Footprint	36 km
Satellite speed	7.0 km/s
Antenna rotating speed	18 rpm
Polarization	VV and HH
Incidence angle range	51.8 deg and 46.7 deg
Antenna pointing angle	44.9 deg and 38.9 deg
Peak transmit power	120 W
WVC resolution	25 km / 12.5 km
Center frequency	13.256 GHz (Ku-band)
Duration of transmit pulse	1.5 ms
Duration of receiving pulse	2.1 ms
Pulse Repetition Frequency (PRF)	96 Hz
Two-way -3dB beam width (azimuth)	1.8 deg
Peak antenna gain	38 dB
Transmit bandwidth	0.375 MHz

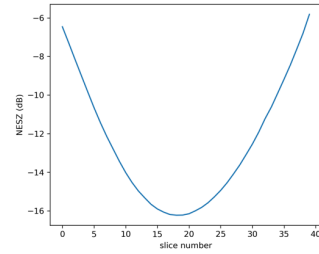
Deleted: 36

Deleted: 4

Deleted: Antenna bandwidth



(a)

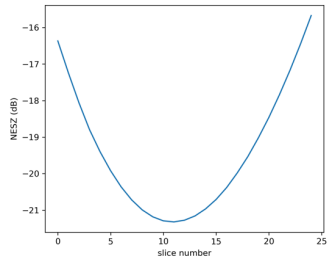


(b)

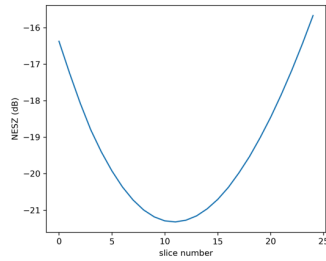
Formatted: Font: Bold

Formatted: Caption

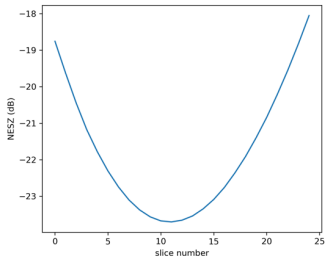
Figure 3: SCAT NESZ distribution as a function of slice number. (a) Ku band HH polarization; (b) Ku band VV polarization.



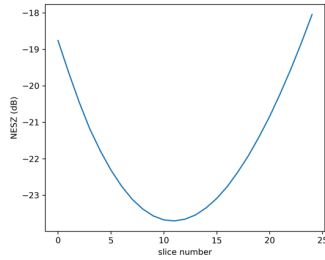
(a)



(b)



(c)



(d)

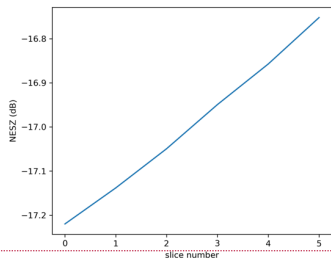
Figure 4: WindRad NESZ distribution as a function of slice number. (a) Ku band HH polarization; (b) Ku band VV polarization; (c) C band HH polarization; (d) C band VV polarization.

Formatted: Font: (Default) +Headings (Times New Roman), Font color: Text 1

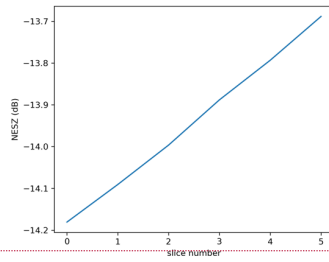
Formatted: Font: (Default) +Headings (Times New Roman), 9 pt, Bold, Font color: Text 1

Formatted: Font: (Default) +Headings (Times New Roman), 9 pt, Bold, Font color: Text 1

Formatted: Font: 9 pt, Bold



(a)



(b)

Figure 5: SeaWinds NESZ distribution as a function of slice number. (a) Ku band HH polarization; (b) Ku band VV polarization.

Formatted: Font: (Default) +Headings (Times New Roman), 9 pt, Font color: Text 1

Formatted: Caption

2.2 Simulation procedure

The simulation is designed to be generic and able to adapt to all of the current rotating-beam wind scatterometers, i.e., both pencil beam and fan beam. It consists of four components: (1) generate satellite state vectors by the orbit propagator SGP4 (Simplified perturbations models) (Hoots and Roehrich, 1980); (2) simulate L1B data; (3) assign the L1B data onto the proper WVCs; (4) aggregate L1B data in one WVC into views (L2A data). The work flow charts are shown in [Figure 6](#) and [Figure 7](#). We use ECMWF model wind as input wind field to initialize the L1B simulation, which provides a spatially smooth ocean wind truth. [In order to simplify the simulation procedure, the pulse is cut into equal size slices](#). To represent the sampling of local wind variability (turbulence), geophysical noise is added by disturbing the input wind components u and v assigned on each slice by injecting Gaussian distributed noise. Together with the instrument configurations and satellite state vectors, the observation geometries on slice level are calculated. The instrument noise K_{pc} (Long et al., 2004) is estimated by $K_{pc}^2 = A + \frac{B}{SNR} + \frac{C}{SNR^2}$. However, the coefficients A, B, and C need onboard processing details, which are not the same nor available for all scatterometers. In order to make the simulator generic, A, B, and C for each slice are calculated by $A = \frac{1}{B_s \times t_d}$, $B = \frac{2}{B_s \times t_r}$, $C = \frac{1}{B_s \times t_r}$, where B_s is the bandwidth for each individual slice, t_d is the transmit duration time, t_r is the receiving time. The distribution of B_s on each slice in one pulse is assigned according to the antenna gain pattern of the pulse.

An example of the simulated satellite orbit together with the location of the slices is given in [Figure 8](#). σ° is derived using the NSCAT-4 GMF for Ku-band and the CMOD5n GMF for C-band and the corresponding beam geometries. Subsequently, the L1B data are obtained after adding the instrument noise on the 'true' σ° . The instrument noise is added by multiplying a Gaussian random number in this way: $\sigma^{\circ}_{noise} = \sigma^\circ \times (1 + K_{pc} \times \text{Gaussian_random_nr})$. The L1B data are assigned to the proper WVCs (Dunbar et al., 2001) and then aggregated into views. A view is a group of slices with similar azimuth angle and the same polarization in one WVC, the properties (i.e. incidence angle, azimuth angle, latitude, longitude, etc.) on the corresponding slices are also aggregated to represent the view (Li et al., 2017). We note that the simulation does currently not include rain effect.

Deleted: 1

Formatted: Font: (Default) Times New Roman, Font color: Auto, English (UK), Snap to grid

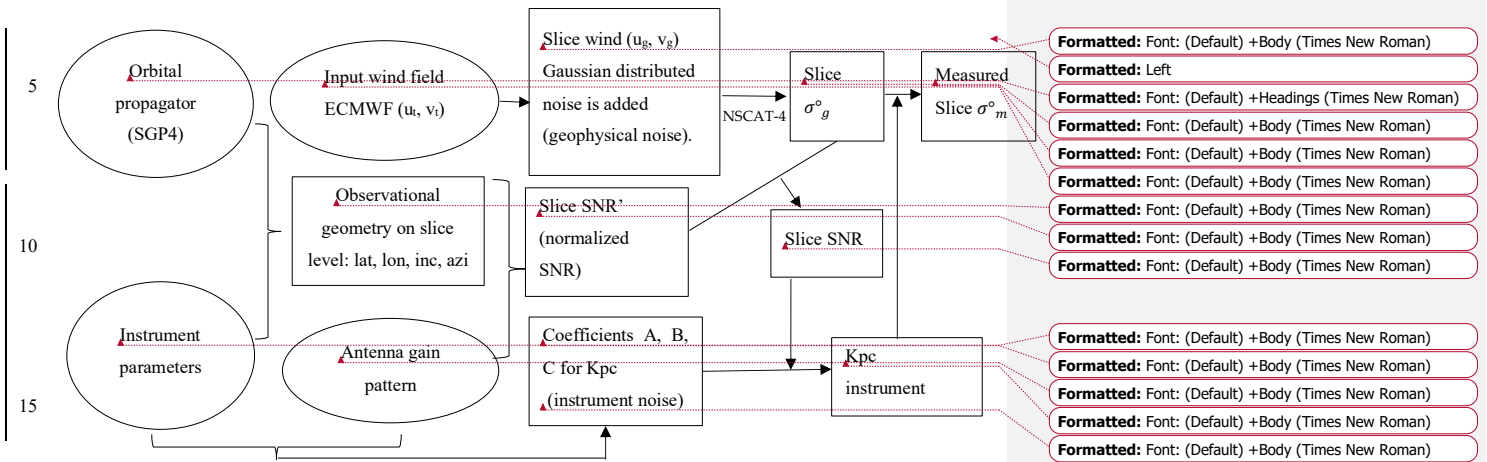
Deleted: Figure 3

Formatted: Font: (Default) Times New Roman, Font color: Auto, English (UK), Snap to grid

Deleted: Figure 4

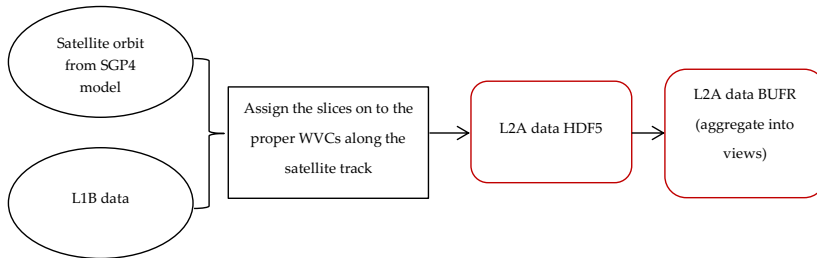
Formatted: Font: (Default) Times New Roman, Font color: Auto, English (UK), Snap to grid

Deleted: Figure 5



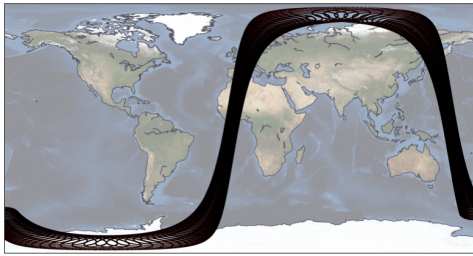
20 **Figure 6:** The workflow for generating L1B simulation data.

Deleted: 3

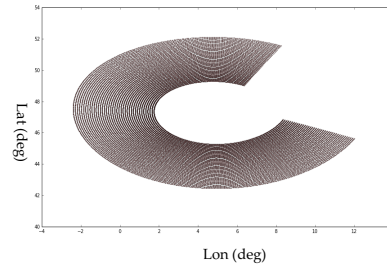


25 **Figure 7:** The workflow to assign L1B data to the proper WVCs and aggregate into views.

Deleted: 4



(a)



(b)

- 5 **Figure 8:** (a) One simulated satellite orbit for CFOSAT starting from 11-12-2011 with the circular motion of the slice located at the end of each pulse; (b) the zoomed in location of all slices on the earth.

Deleted: 5

2.3 Wind field retrieval principle

The Maximum Likelihood Estimator (MLE) is the most classic algorithm for wind retrieval. It has been applied in many wind retrieval studies (Chi and Li, 1988; JPL, 2001; Pierson, 1989; Portabella and Stoffelen, 2002). We adopted it and applied it in our wind retrievals. The MLE can be expressed as (JPL, 2001):

$$MLE = \frac{1}{N} \sum_{i=1}^N \left(\frac{\sigma_{mi}^{\circ} - \sigma_{si}^{\circ}}{Kp(\sigma_{xi}^{\circ})} \right)^2 \quad (1)$$

where N is the number of views, and σ_{xi}° is either σ_{mi}° (measured σ°) or σ_{si}° (trial simulated σ°). $Kp(\sigma_{xi}^{\circ})$ is the expected Gaussian observation noise with the form of $Kp \times \sigma_{xi}^{\circ}$. The wind inversion procedure takes L2A data and searches for the σ_{si}° with minimum MLE by varying trial wind speeds and directions. The σ_{si}° with the minimum MLE is known as the first rank solution. However, the first solution is often not the best solution because the wind retrieval results usually consist of a set of ambiguous solutions due to the combination of measurement geometry, the harmonic modulation of the GMF (non-linear GMF), noise, etc. After the wind retrieval step, one of the ambiguous solutions is selected by the Two-Dimensional Variational Ambiguity Removal (2DVAR) (Vogelzang, 2013) after minimizing a total cost function that combines both observational and NWP background contributions. The retrieved wind field can be compared with the input wind field to assess the wind retrieval quality.

20 2.4 Simulation assessment

Deleted: 3

2.4.1 Simulation model validation

SeaWinds is chosen as the validation data in comparison with simulated data since it has worked about 10 years and the other two scatterometers do not have sufficient data. All the scatterometers' simulation orbit is the same as CFOSAT in order to have a good inter-comparison among the three scatterometers and it is different from the actual orbit of SeaWinds, so there are in total 77866 collocated WVCs (one day 14 orbits data) and Figure 9 shows the collocated wind retrieval result. The simulated wind speed and wind direction give a good correlation to the real SeaWinds data, which means the simulation model has good performance, and it is suitable for the comparison among the different type of scatterometers.

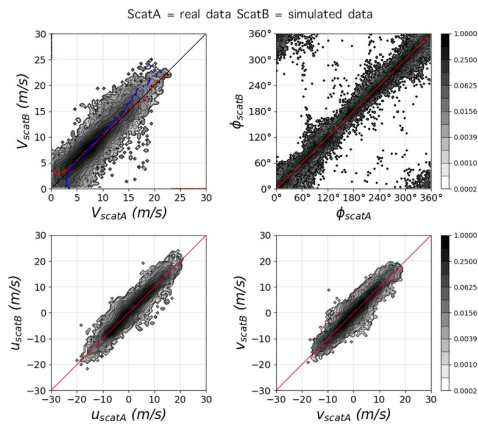


Figure 9: The collocation between SeaWinds (ScatA) and simulated SeaWinds (ScatB) in wind speed (upper left), wind direction (upper right), u component (lower left), v component (lower right).

2.4.2 SCAT, WindRad, and SeaWinds view number comparison

The most important differences between SCAT, WindRad, and SeaWinds are the shape of the antenna and the number of antennas, directly leading to a different distribution of the number of views across the swath. SeaWinds as rotating pencil-beam instrument has 4 views in each WVC across the swath, where the fore and aft views in the outer swath are each split in two views. The number of slices in each view varies across the swath though. For rotating fan-beam instruments, the view number varies across the swath with the feature of less views in the outer and nadir swath, and more views in the parts of the swath in between (Figure 10). It can be observed that both SCAT and WindRad contain more views than SeaWinds for all WVCs, with a saddle shape in the view count. Moreover, the number of views of WindRad is about twice the number of views of SCAT.

Formatted: Font: Not Bold

Formatted: Justified, Indent: First line: 0.31", Line spacing: 1.5 lines

Formatted: Font: Times New Roman, Not Italic, Font color: Auto, English (UK), Check spelling and grammar, Snap to grid

Formatted: Indent: First line: 0"

Formatted: Caption, Indent: First line: 0"

Formatted: Font: Not Bold

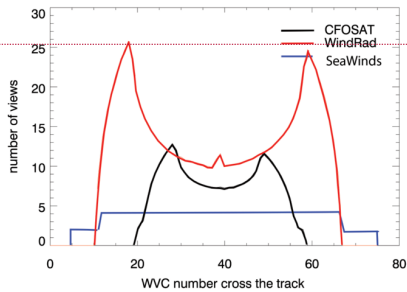
Formatted: Indent: First line: 0.31"

Deleted: 3

Deleted: 1

Formatted: Font: (Default) Times New Roman, Font color: Auto, English (UK), Snap to grid

Deleted: Figure 6



Deleted: <object>

15 **Figure 10.** Averaged number of views at the WVCs across the swath.

Deleted: 6

Deleted: ¶
Deleted: ¶

Formatted: Caption

Deleted: 3

Deleted: 2

2.4.3 Instrument noise

The instrument noise (Kpc) of the simulator for SCAT, WindRad and SeaWinds are estimated at various wind speed (4 m/s, 9 m/s, and 16 m/s) on slice level and WVC level. The Kpc for each view is aggregated by weighting the Kpc of the slices in this view and the Kpc on WVC level is derived by averaging the Kpc for all the views in the corresponding WVC.

25 Figure 11(a) shows the slice Kpc of SCAT as a function of incidence angle. The slices with high wind speed and high incidence angle contain high Kpc and Kpc for VV polarization overall is lower than for HH, except for the slices with incidence angle lower than 30.25° (indicated by the dashed line in Figure 11(a)). The Kpc in a WVC for SCAT (Figure 11(c)) is much lower than the Kpc on slice level, as expected due to the aggregation of the slices in a WVC. The outer swath contains relatively high instrument noise as compared to sweet and nadir swath. Low wind speed leads to a higher Kpc. On the WVC level, the instrument noise is lower than 20% except for low wind speed.

Deleted: Figure 7

Formatted: Font: (Default) Times New Roman, Font color: Auto

Formatted: Font: (Default) Times New Roman, Font color: Auto

Deleted: Figure 7

Formatted: Font: (Default) Times New Roman, Font color: Auto

Deleted: Figure 7

30 WindRad has two frequencies at Ku and C band. As illustrated in Figure 12(a) and (b), the VV Kpc is lower than the HH Kpc for Ku and C band and the C-band Kpc is much lower than the Ku-band Kpc. On the WVC level (Figure 12(c)), it shows a similar pattern to SCAT and generally the instrument noise is lower than 10% if the outer swath and low wind speeds are excluded.

Formatted: Font: (Default) Times New Roman, 10 pt, Not Bold, Font color: Auto

Deleted: Figure 8

Deleted: Figure 8

35 The SeaWinds Kpc on slice level (Figure 13(a) (b)) is more constant at wind speed of 9m/s and 16m/s, while it is increasing along with the incidence angle at low wind speed 4m/s. On WVC level, the Kpc is lower than 20% except for wind speeds below 4m/s. We note that a random error of 20% at 4 m/s is still acceptable in terms of absolute random wind error after wind retrieval.

Formatted: Font: (Default) Times New Roman, 10 pt, Not Bold, Font color: Auto

Formatted: Font: (Default) Times New Roman, Font color: Auto

Deleted: Figure 9

In general, low wind speeds cause high instrument noise, as expected, and the instrument noise on WVC level is less than 20% for SCAT, less than 10% for WindRad and less than 20% for SeaWinds, when the outer swath and low wind

speeds are excluded. All scatterometers above have a pattern of higher Kpc at the outer swath as compared to the other parts of the swath.

2.4.4 1st rank wind retrieval and 2DVAR performances

5 As already known, the first rank solution is not always the best solution, but the more often the first rank solutions are chosen to be the best solution, the lower the ambiguity in the inverted instrument wind solutions. The quality of the 1st rank solution thus reflects the ambiguity in the wind measurement system. So, it is chosen for the comparison of the wind retrieval performance on SCAT, WindRad, and SeaWinds. The difference between 1st rank solution and 2DVAR performance provides insight in the effects of the wind direction ambiguities on the final selected wind field, which may
10 depend on measurement geometry. 2DVAR with MSS (Multiple Solution Scheme) (Vogelzang, 2013) has been applied in our simulation. A weighted analysis field is constructed by combining the scatterometer observations and a model prediction, and then the one lying closest to the analysis field is selected as the output solution. The problem is solved by minimizing a total cost function that combines both observation and NWP information: $J = J_{obs} + J_{NWP} = -2[\ln P(\mathbf{v}_k|\mathbf{x}) + \ln P(\mathbf{x}|\mathbf{x}_b)]$, where \mathbf{x} is the true state of the surface wind field, \mathbf{v}_k is the possible ambiguous wind solutions, $P(\mathbf{v}_k|\mathbf{x})$ is the conditional
15 probability of the \mathbf{v}_k observed given \mathbf{x} , and $P(\mathbf{x}|\mathbf{x}_b)$ is the conditional probability of surface wind field \mathbf{x} given \mathbf{x}_b . Detail of the method can be found in [21,22,23].

A statistical comparison of 1st rank solution and 2DVAR performances of SCAT, WindRad, and SeaWinds are shown in [Figure 14](#), [Figure 15](#), [Figure 16](#). For SCAT, the 1st rank solution wind field ([Figure 14](#)(a)) shows poor retrieval quality in the nadir and outer swath, while 2DVAR ([Figure 14](#)(b)) effectively improves the retrieval results here; by the way a similar
20 effect occurs for SeaWinds ([Figure 16](#)). The nadir swath of WindRad shows worse wind retrieval quality than the other parts of the swath ([Figure 15](#)(a)) and 2DVAR is able to correct the false solutions appearing in the 1st rank solution. Note that the rotation sampling pattern of WindRad is visible as regular disturbances along the swath. This implies that for the same WVC number, different sets of views are collected, depending on the phase of the antenna rotation, hence the wind retrieval performance may vary, e.g., the expected MLE. One aspect needs to be noted: the 2DVAR with MSS works properly in our
25 simulation, but the input wind field of the simulation is ECMWF model data, which is consistent with the 2DVAR background field. Even though a Gaussian-distributed geophysical noise has been added in the input wind field, it still might lead to a selection of wind solutions that tends to be close to the model wind field and hence somewhat overestimates performance.

30

Deleted: 3

Deleted: 3

Deleted: Figure 10

Deleted: Figure 11

Deleted: Figure 12

Deleted: Figure 10

Formatted: Font: (Default) Times New Roman, Font color: Auto, English (UK), Snap to grid

Formatted: Font: (Default) Times New Roman, Font color: Auto, English (UK), Snap to grid

Formatted: Font: (Default) Times New Roman, Font color: Auto, English (UK), Snap to grid

Formatted: Font: (Default) Times New Roman, Font color: Auto, English (UK), Snap to grid

Formatted: Font: (Default) Times New Roman, Font color: Auto, English (UK), Snap to grid

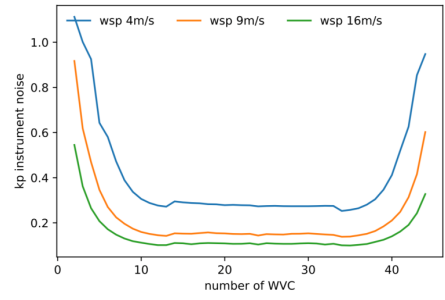
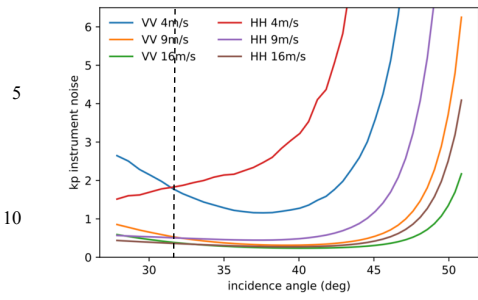
Deleted: Figure 10

Formatted: Font: (Default) Times New Roman, Font color: Auto, English (UK), Snap to grid

Deleted: Figure 12

Deleted: Figure 11

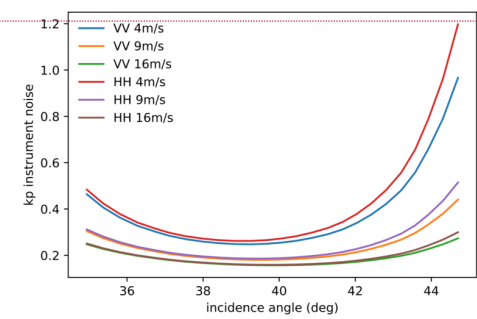
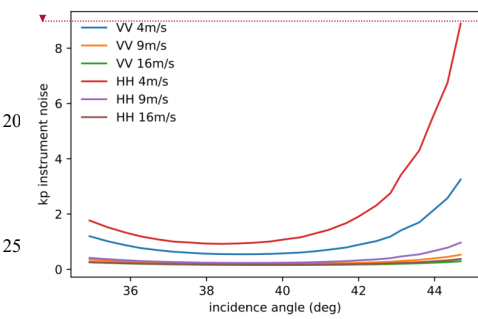
Formatted: Font: (Default) Times New Roman, Font color: Auto, English (UK), Snap to grid



(a)

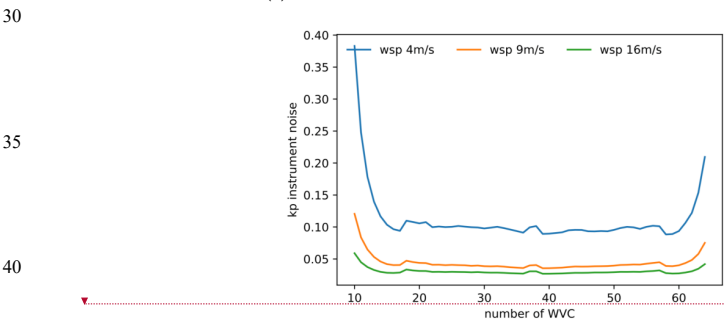
(b)

15 **Figure 11:** SCAT instrument noise in ratio (1 is 100%) at 4m/s, 9m/s, and 16 m/s on (a) slice level; (b) WVC mean K_p .



(a)

(b)

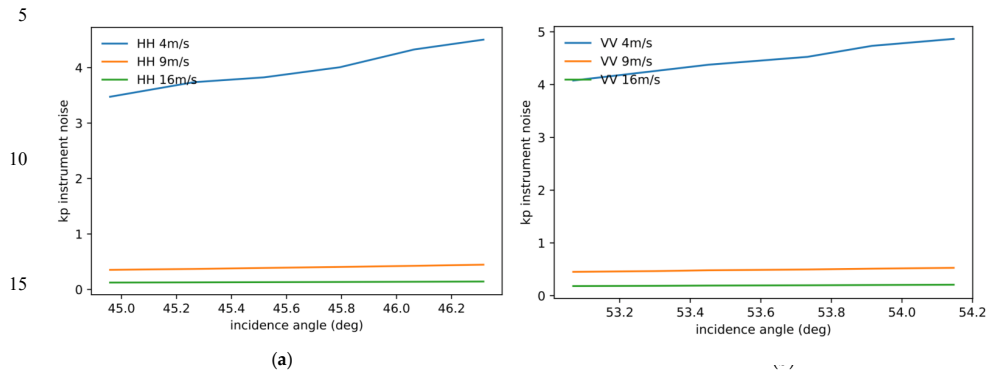


Deleted: 7
 Deleted: p.
 Formatted: Font: Bold
 Deleted: ¶
 Deleted: ¶
 Deleted: ¶

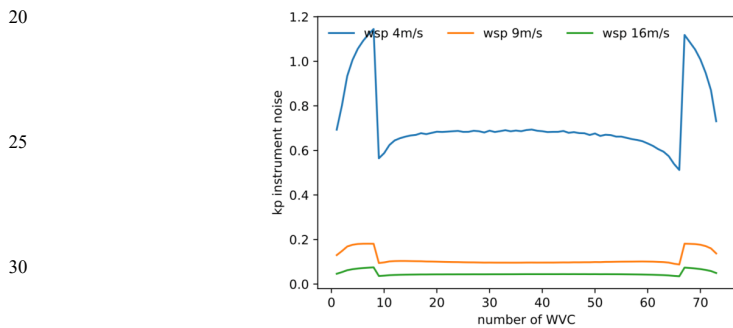
Deleted: ¶
 Formatted: Indent: First line: 0"

(c)

Figure 12: WindRad instrument noise in ratio (1 is 100%) at 4m/s, 9m/s, and 16 m/s on (a) slice level of Ku-band; (b) slice level of C-band (slices with SNR < 0.05 are excluded); (c) WVC mean Kp.



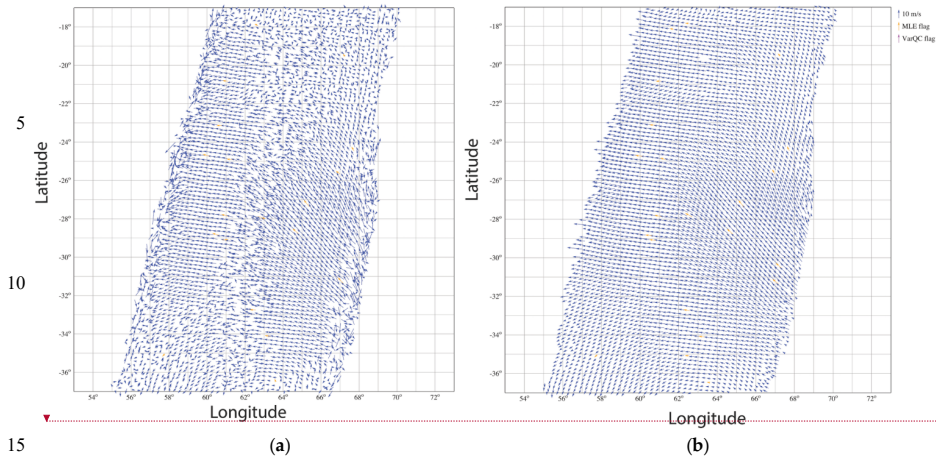
(a)



(c)

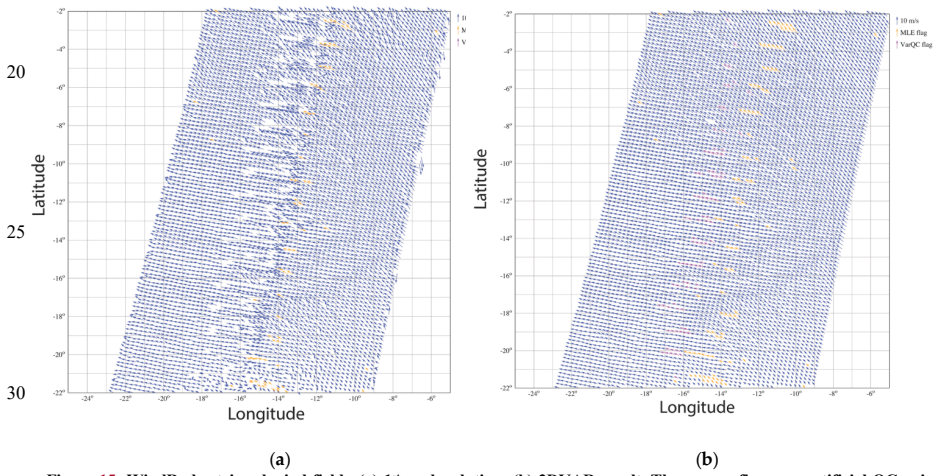
Figure 13: SeaWinds instrument noise in ratio (1 is 100%) at 4m/s, 9m/s, and 16 m/s on (a) slice level of Ku-band HH pol; (b) slice level of Ku-band VV pol (slices with SNR < 0.05 are excluded); (c) WVC mean Kp.





Deleted: 1

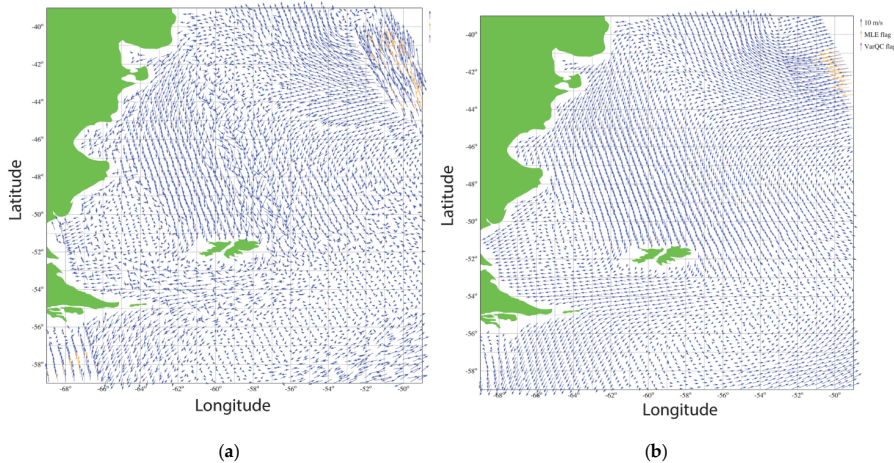
Deleted: 10



Deleted: 11

35

5



10

15

Figure 16: SeaWinds retrieved wind field. (a) 1st rank solution; (b) 2DVAR result. The orange flags are artificial QC points and may be ignored.

Deleted: 12

Formatted: Caption

Deleted: ¶

3. Simulation result and wind retrieval performance comparison

20

The simulation has been performed on SCAT, WindRad and SeaWinds with ECMWF model wind data (17th Dec, 2011) as input wind field. The swath widths for the three instruments are different, in order to make the following figures more comparable, the nadir WVCs of the three instruments are aligned.

3.1 Wind retrieval performance evaluation

3.1.1 Assessments with the input wind field

25

Four orbits of data on 2011-12-17 have been generated to be used for the wind retrieval simulation. The contoured histograms in [Figure 17](#), [Figure 18](#) and [Figure 19](#) provide statistics of the wind speed, wind direction with respect to a wind blowing from the North, and wind components u (eastward) and v (northward) versus the variable “true” input wind field for SCAT, WindRad and SeaWinds. We note that opposing wind solutions will have opposite u and v signs and similar amplitude and therefore such common ambiguity appears as a cross pattern in the u and v histograms. This ambiguity is directly related to the main double harmonic dependency of the GMF (Wang et al., submitted, 2018).

30

For SCAT ([Figure 17](#), (a)), the 1st rank solution of all WVCs across the swath are included. It shows rather poor statistics when compared with the input wind field. However, by simply excluding the WVCs located in the outer swath, the 1st rank solution quality improves substantially ([Figure 17](#), (b)). The spread in the wind speeds is reduced and some derived

Formatted: Font: (Default) Times New Roman, 10 pt, Not Bold, Font color: Auto, English (UK), Snap to grid

Deleted: Figure 13

Formatted: Font: (Default) Times New Roman, 10 pt, Not Bold, Font color: Auto, English (UK), Snap to grid

Deleted: Figure 14

Formatted: Font: (Default) Times New Roman, 10 pt, Not Bold, Font color: Auto, English (UK), Snap to grid

Deleted: Figure 15

Formatted: Font: (Default) Times New Roman, 10 pt, Not Bold, Font color: Auto, English (UK), Snap to grid

Deleted: Figure 13

Formatted: Font: (Default) Times New Roman, 10 pt, Not Bold, Font color: Auto, English (UK), Snap to grid

Deleted: Figure 13

false wind directions, which are shown as parallel and perpendicular lobes to the true value in the plots, are removed. When the nadir-swath WVCs are also excluded (Figure 17(c)), then the wind speed collocation statistics stay almost unchanged as compared to Figure 17b, while most of the false wind directions perpendicular to the true value are removed. This means that the outer swath contains the most ambiguous wind vector results, while the nadir swath ambiguities cause mainly wind direction errors.

Figure 18(a) shows the 1st rank wind retrieval for WindRad with all WVCs and it shows much better statistics as compared to SCAT (Figure 17(a)), due to twice the number of views in each WVC. Excluding outer WVCs (Figure 18(b)) has less effect on the wind retrieval quality for WindRad than for SCAT. The retrieved wind speed shows a bit better statistic, but wind direction statistics stay almost unchanged, which means that the outer WVCs do not strongly increase the wind direction ambiguity. On the other hand, when we only exclude nadir WVCs (Figure 18c), the wind direction retrieval is improved. The average wind speed bias is 0.42 m/s and the standard deviation of wind direction is 32.21° (Figure 18(c)), while they are 0.51 m/s and 41.30° for Figure 18(b), respectively. The last experiment shown for WindRad is to exclude both outer and nadir WVCs (Figure 18(d)) with averaged wind speed bias of 0.44 m/s and standard deviation of wind direction of 35.61°. The largest performance improvement of WindRad occurs when excluding nadir WVCs. The outer swath mainly influences the wind speed retrieval skill, while the nadir swath provides wind direction ambiguity.

SeaWinds's outer swath contains only two views (fore-VV and aft-VV), and in order to process outer swath winds, each of these two views are split into two views based on their azimuth angle (four views in total in the end). Even though there are four views at the outer swath, the limited azimuth diversity leads to more ambiguous wind retrieval results (Figure 19). The wind retrieval quality of SeaWinds is the poorest one among these three instruments.

The averaged wind retrieval statistics against the input wind field are dominated by the lack of ambiguity removal and non-linearity. In practice these issues are successfully dealt with in the ambiguity removal step, using prior background information. In next section we determine Figures of Merit (FoM) to compare scatterometer performances with and without such prior information.

Formatted: Font: (Default) Times New Roman, 10 pt, Not Bold, Font color: Auto, English (UK), Snap to grid

Deleted: Figure 13

Deleted: Figure 13

Formatted: Font: (Default) Times New Roman, 10 pt, Not Bold, Font color: Auto, English (UK), Snap to grid

Formatted: Font: (Default) Times New Roman, 10 pt, Not Bold, Font color: Auto, English (UK), Snap to grid

Deleted: Figure 14

Deleted: Figure 13

Formatted: Font: (Default) Times New Roman, 10 pt, Not Bold, Font color: Auto, English (UK), Snap to grid

Deleted: Figure 14

Formatted: Font: (Default) Times New Roman, 10 pt, Not Bold, Font color: Auto, English (UK), Snap to grid

Formatted: Font: (Default) Times New Roman, 10 pt, Not Bold, Font color: Auto, English (UK), Snap to grid

Deleted: Figure 14

Formatted: Font: (Default) Times New Roman, 10 pt, Not Bold, Font color: Auto, English (UK), Snap to grid

Deleted: Figure 14

Deleted: Figure 14

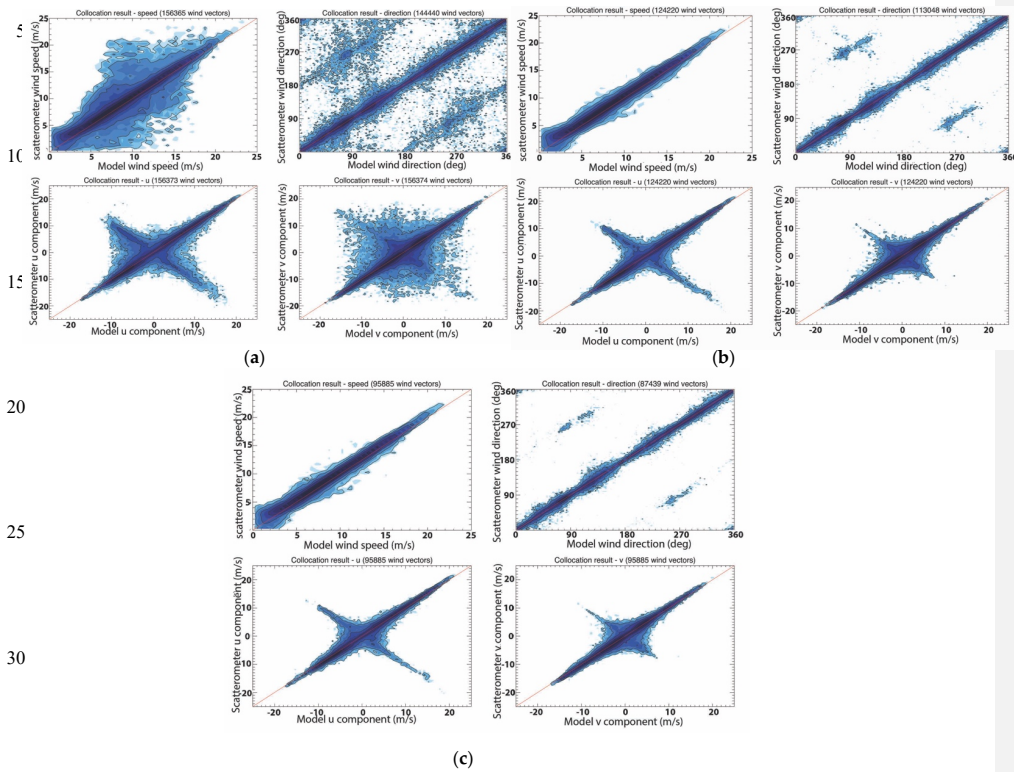
Formatted: Font: (Default) Times New Roman, 10 pt, Not Bold, Font color: Auto, English (UK), Snap to grid

Formatted: Font: (Default) Times New Roman, 10 pt, Not Bold, Font color: Auto, English (UK), Snap to grid

Deleted: Figure 14

Formatted: Font: (Default) Times New Roman, 10 pt, Not Bold, Font color: Auto, English (UK), Snap to grid

Deleted: Figure 15



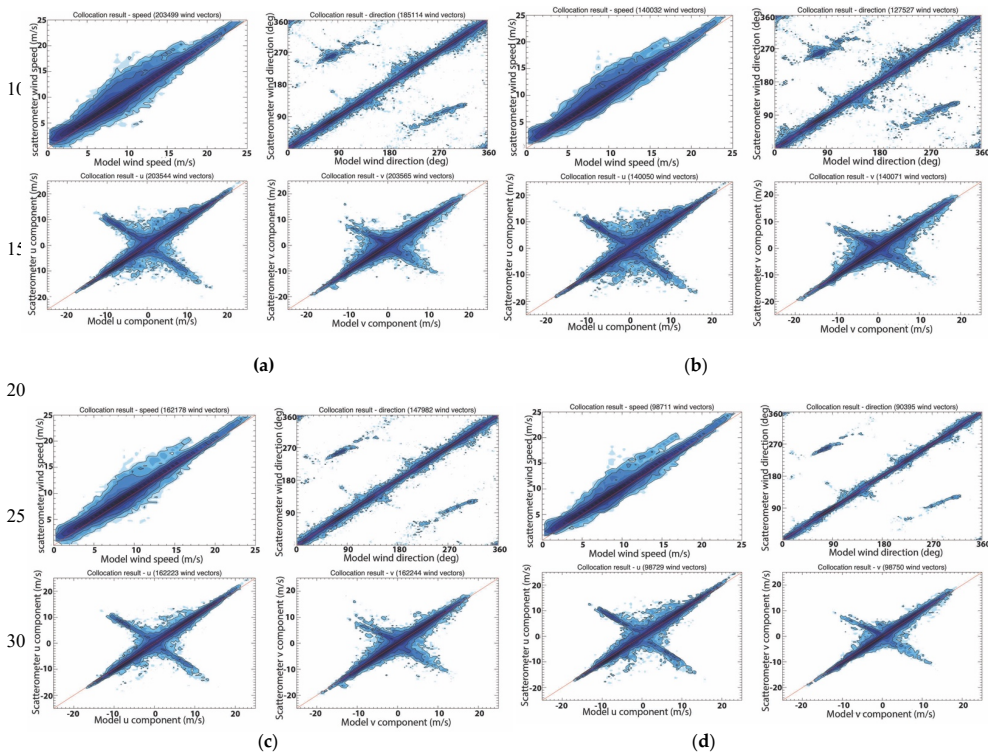
Deleted: ¶

Deleted: ¶

Deleted: 13

Figure 17: Contoured histograms of SCAT retrieved 1st rank wind solution versus input wind field for 4 orbits. (a) all WVCs within the swath; (b) excluding the WVCs in the outer swath, WVC number from 8 to 42 are included; (c) excluding the WVCs in the outer swath and nadir swath, WVC number from 8 to 17 and 26 to 42 are included. From (a) to (c), upper left: wind speed; upper right: wind direction; lower left: u component; lower right: v component. The contour lines are logarithmic.

5



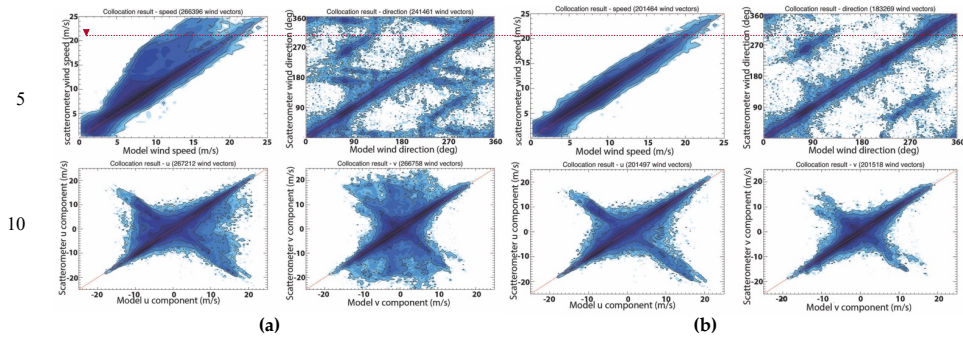
35

Figure 18: Contoured histograms of WindRad retrieved 1st rank wind solution versus input wind field for 4 orbits. (a) all WVCs within the swath; (b) excluding the WVCs in the outer swath, WVC number from 20 to 60 are included; (c) excluding the WVCs in the nadir swath, WVC number from 35 to 45 are included; (d) excluding the WVCs in the outer swath and nadir swath, WVC number from 20 to 35 and 45 to 60 are included. The four figures in (a-d), upper left: wind speed; upper right: wind direction; lower left: u component; lower right: v component. The contour lines are logarithmic.

40

Deleted: 14

Deleted: 1



15 **Figure 19:** Contoured histograms of SeaWinds retrieved 1st rank wind solution versus input wind field for 4 orbits. (a) all WVCs within the swath; (b) excluding the WVCs in the outer swath, WVC numbers from 10 to 65 are included. From (a) to (b), upper left: wind speed; upper right: wind direction; lower left: u component; lower right: v component. The contour lines are logarithmic.

Deleted: <object><object>

Formatted: MDPI_3.1_text

Deleted: 15

Deleted: ¶

3.1.2 Figure of Merits

20 The 1st rank solutions contain ambiguities and because the input wind field is the ECMWF model wind, but without spatially correlated error, it leads to a nearly perfect 2DVAR result, which is unrealistic. In order to further evaluate the wind retrieval performance, the ambiguity of the solutions may be statistically evaluated in the context of generally available background (NWP) information. Figures of Merit (FoM) are a set of parameters to evaluate the wind retrieval quality of different scatterometer concepts, taking into account imprecise, ambiguous and biased wind solutions. Three FoM, which are

25 normalized wind Vector RMS error (VRMS), Ambiguity Susceptibility (AMBI) and systematic error (BIAS), are introduced here based on (Rivas et al., 2009). A brief description is given first.

The VRMS FoM is defined to quantify the ability of the scatterometer wind retrieval to handle ambiguous solutions with a priori NWP model information, such as in 2DVAR, but without actually simulating realistic spatially correlated errors. The input wind field to our simulation is considered as true winds (denoted with \mathbf{v}_T). VRMS quantifies the total

30 simulated wind retrieval error with respect to \mathbf{v}_T . It is, however, calculated by down-weighting ambiguous wind vector solutions that are very distant from \mathbf{v}_T , since in practice it is easiest for 2DVAR and other applications to discard such solutions. The down-weighting involves the common prior knowledge in these applications, which is the general NWP background wind component uncertainty, denoted σ_{NWP} and assumed equal for u and v. The ambiguous retrieved wind vector distribution, expressed in the wind probability $P_{obs}(\mathbf{v}|\mathbf{v}_T)$, is multiplied by a Gaussian probability distribution

35 $P_{NWP}(\mathbf{v} - \mathbf{v}_T)$ centered at the input wind field and with a variance $\sigma_{NWP}^2 \sim 5 \text{ m}^2/\text{s}^2$ in both wind components. The VRMS FoM is subsequently obtained by normalizing this expression by the prior NWP VRMS error:

$$FoM_{VRMS} = \frac{RMS_{obs}}{RMS_{NWP}} \quad (2)$$

where $RMS_{obs} = \left(\int \int |\mathbf{v} - \mathbf{v}_t|^2 P_{obs}(\mathbf{v}|\mathbf{v}_t) \times P_{NWP}(\mathbf{v} - \mathbf{v}_t) d^2v \right)^{1/2}$ and $RMS_{NWP} = \left(\int \int |\mathbf{v} - \mathbf{v}_t|^2 P_{NWP}(\mathbf{v} - \mathbf{v}_t) d^2v \right)^{1/2} = \sqrt{2}\sigma_{NWP}$. VRMS quantifies the wind solution's relative RMS about the true wind with respect to the general prior background uncertainty. If its value is 1, then the wind retrieval failed to provide new and useful information in the wind field, i.e., corresponding to $P_{obs}(\mathbf{v}|\mathbf{v}_t) = \text{constant}$.

5 On the other hand, AMBI is defined to quantify the ability of the scatterometer and its processing to handle ambiguous solutions without a priori NWP model information. It is a ratio of the wind solution output falling outside the general prior wind field constraint, relative to the output falling inside the prior wind field constraint. The lower the ratio, the better (3), where $P_{NWP,max}$ is the maximum probability of $P_{NWP}(\mathbf{v} - \mathbf{v}_t)$.

$$FoM_{AMBI} = \frac{\int P_{obs}(\mathbf{v}|\mathbf{v}_t) \times (P_{NWP,max} - P_{NWP}(\mathbf{v} - \mathbf{v}_t)) d^2v}{\int P_{obs}(\mathbf{v}|\mathbf{v}_t) \times P_{NWP}(\mathbf{v} - \mathbf{v}_t) d^2v} \quad (3)$$

10 BIAS quantifies the systematic vector wind bias, again in the context of the background prior, which is the shift of the average location of the output wind solution away from the location of the prior wind caused by skewness in the output wind solutions (4).

$$FoM_{BIAS} = \int (\mathbf{v} - \mathbf{v}_t) \cdot P_{obs}(\mathbf{v}|\mathbf{v}_t) \times P_{NWP}(\mathbf{v} - \mathbf{v}_t) d^2v \quad (4)$$

The wind retrieval is a non-linear problem and the output wind error depends on the true wind vector (wind speed and direction distribution). In order to minimize this dependence, the calculated FoMs are averaged over a climatology of wind inputs with uniformly distributed directions and wind speeds (3 m/s to 16 m/s) following a Weibull distribution with a maximum around 8 m/s (Liu et al., 2008). The input wind speeds are from 3 to 16 m/s with steps of 1 m/s, and the input wind directions are from 0 to 360 degrees with steps of 10 degrees. Each wind speed and wind direction combination contains the equivalent number of WVCs from the same orbit.

20 **Figure 20** gives the three FoM comparisons of SCAT, WindRad and SeaWinds as a function of the WVC positions in the swath. Overall, the wind retrieval performance of the rotating fan-beam instruments is better than the pencil-beam instrument, while the outer and nadir swaths of the three instrument types yield a poorer performance than the sweet swaths. The outer swath of SeaWinds only has two independent views, which result in very ambiguous winds and the worst simulated wind retrieval quality. The wind retrieval quality across the swath strongly depends on the location of the WVC; it degrades substantially in the outer and nadir swaths as expected. The outer swath has worse quality than the nadir swath for both SCAT and SeaWinds, whereas these two regions are showing comparable wind retrieval quality for WindRad.

Formatted: Font: (Default) Times New Roman, 10 pt, Not Bold, Font color: Auto, English (UK), Snap to grid

Deleted: Figure 16

Although the number of views in the sweet swath for WindRad is twice the number for SCAT (Figure 10), the wind retrieval quality is not improved as expected, but shows very similar quality to SCAT. The elevated values for AMBI and BIAS indicate that, despite the high number of views, the wind retrieval tends to be not well determined and slightly non-linear. At the same time, the quality in the outer swath of WindRad shows very pronounced improvement with respect to SCAT, due to the increased number of available views.

Figure 21 illustrates the VRMS as a function of wind direction and WVC location at 9 m/s wind speed. The wind retrieval performance across the swath for all wind directions gives the same pattern as described above with some modulations at different wind direction. There is one different feature occurring for WindRad. The VRMS at nadir swath shows higher values than in the outer swath, which is opposite to SCAT and SeaWinds. AMBI and BIAS (not shown here) have similar patterns as VRMS.

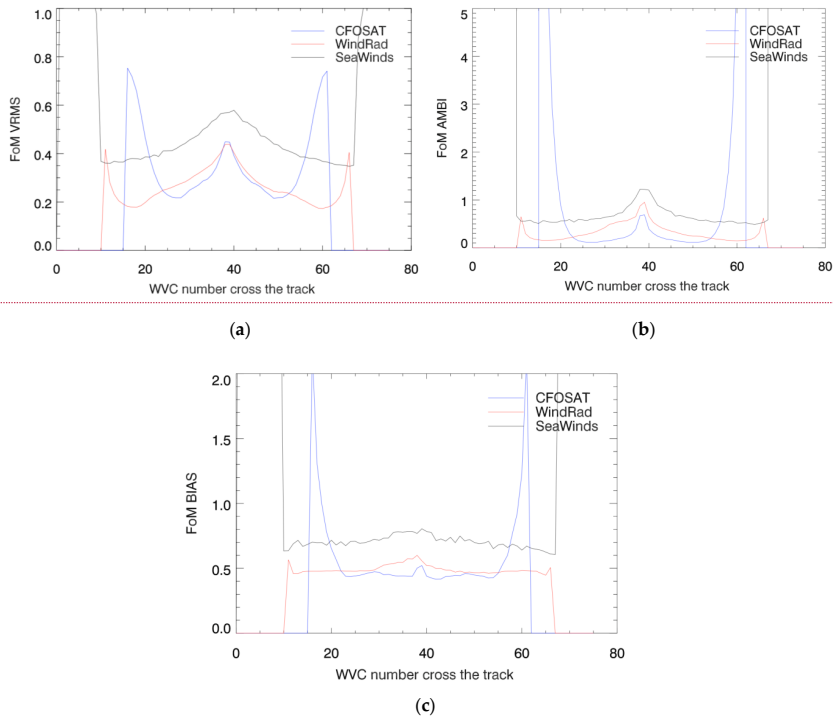


Figure 20: FoM results of SCAT, WindRad, and SeaWinds. (a) VRMS comparison; (b) AMBI comparison; (c) BIAS comparison.

Deleted: Figure 6

Formatted: Font: (Default) Times New Roman, Font color: Auto, English (UK), Snap to grid

Deleted: Figure 17

Formatted: Font: (Default) Times New Roman, 10 pt, Not Bold, Font color: Auto, English (UK), Snap to grid

Deleted: ¶

Deleted: 16

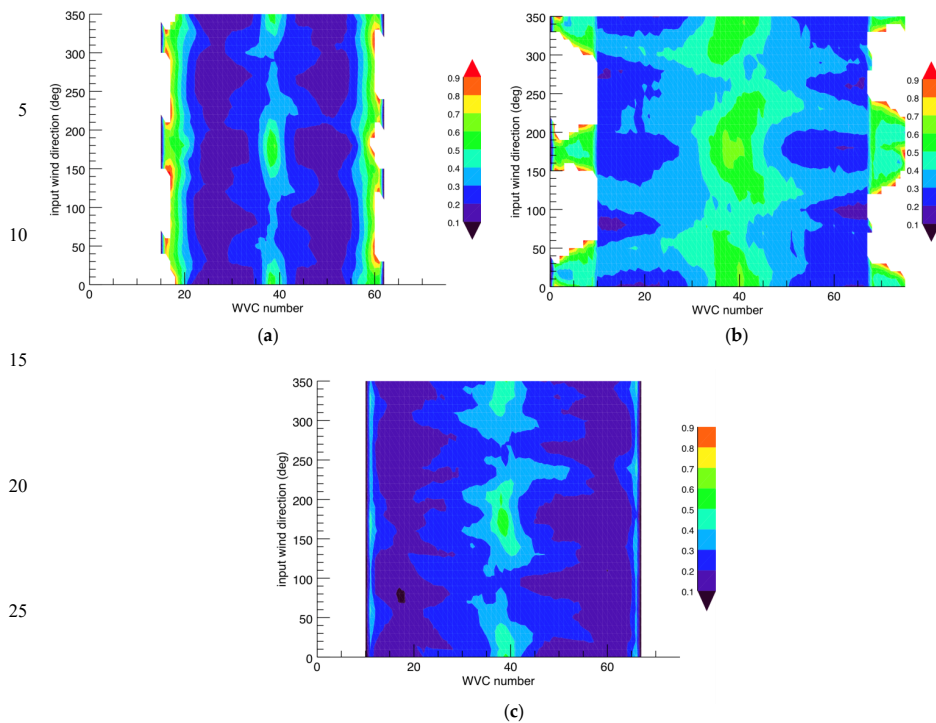


Figure 21: FOM VRMS map as a function of across-track location and wind direction (wind speed is 9 m/s). (a) SCAT; (b) SeaWinds; (c) WindRad.

Deleted: 17

3.1.3 Wind direction bias

Wind direction bias between the wind retrieval result (2DVAR result) and the ECMWF model wind has been evaluated as a function of WVC and relative wind direction (15 orbits are included). The relative wind direction means the retrieved wind direction relative to the satellite motion direction. In this evaluation, we are able to see the wind direction bias with respect to the true direction at all the WVCs (Figure 22). No matter the biases are negative or positive, both signs indicate that the wind directions have a tendency to be closer to the satellite motion direction and if the wind direction bias is averaged over all the relative wind directions, a small value of the bias remains.

Formatted: Font: (Default) Times New Roman, 10 pt, Not Bold, Font color: Auto, English (UK), Snap to grid

Deleted: Figure 18

SeaWinds gives stronger bias both on the outer swath and nadir swath (Figure 22 (b)), while the nadir swath of SCAT gives weaker bias comparing to the outer swath due to the increased number of views (Figure 22 (a)). For WindRad, when the retrieved wind direction is close to satellite motion direction (relative wind direction is 0), it shows rather strong negative and positive bias, but the non-biased area for WindRad is larger than it is in SCAT and SeaWinds. This phenomena can also be observed with real data from SCATSAT (Wang et al., submitted, 2018). This retrieved wind direction preference might be caused by the retrieval method.

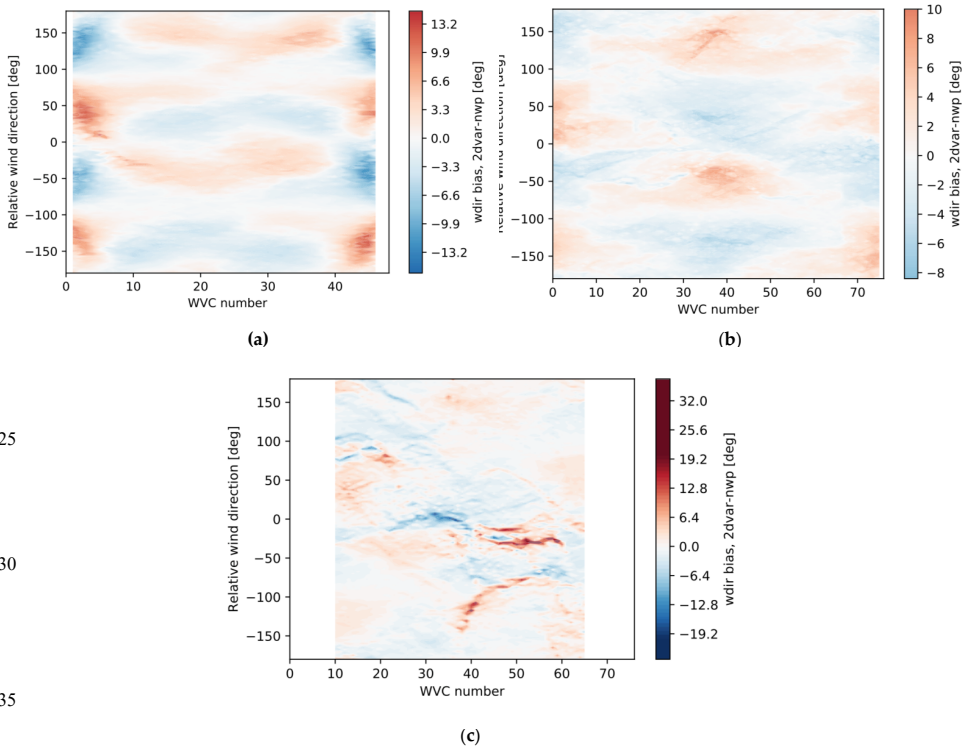


Figure 22: Wind direction bias between wind retrieval result and true wind as a function of WVC number and the relative wind direction (y-axis, the retrieved wind direction relative to the satellite motion direction; color scale is consistent for easy comparison, all the values outside [-20, 20] are marked as dark blue and dark red). (a) SCAT; (b) SeaWinds; (c) WindRad.

Deleted: Figure 18

Formatted: Font: (Default) Times New Roman, 10 pt, Not Bold, Font color: Auto, English (UK), Snap to grid

Deleted: Figure 18

Formatted: Font: (Default) Times New Roman, 10 pt, Not Bold, Font color: Auto, English (UK), Snap to grid

Deleted: 18

4. Discussion

Our results confirm that the wind retrieval quality of Ku-band rotating-beam scatterometers (rotating fan-beam and rotating pencil-beam) varies according to the location of the WVCs across the swath, and the outer and nadir swaths show generally lower wind retrieval skill than the sweet swath. The wind retrieval comparisons suggest that WindRad gives the best wind retrieval quality of the three scatterometer types, although its increased number of views not always lead to further wind retrieval quality improvement, particularly in the sweet swath.

Prior work on SCAT and WindRad mainly focused on the instrument configuration choices and tests with various settings of pulse frequency, polarization, rotating speed, transmitted peak power, etc. (Lin et al., 2000a, 2002; Lin and Dong, 2011). The main wind retrieval performance characteristics of these two-rotating fan-beam scatterometers are in line with our study with respect to sweet swath, nadir and outer swath performance. SCAT has been compared with SeaWinds (Lin and Dong, 2011) in an end-to-end simulation and now we add a cross comparison among SCAT, WindRad and SeaWinds in the same simulation framework as before.

WindRad shows distinguished and new wind retrieval features in our study with respect to SCAT and SeaWinds. The outer swaths of SCAT and SeaWinds clearly provide the worst wind retrieval skill as compared to nadir, but for WindRad this does not occur. WindRad gives very similar wind retrieval quality in the nadir and outer swaths according to its FoM (Figure 20). However, the spread of the FoM values are largest in the inner swath (Figure 21) and excluding the inner swath leads to a better wind retrieval instead of excluding the outer swath. This is opposite to SCAT and SeaWinds, where performance increases most when excluding the outer swath.

Increasing the number of views and azimuth diversity leads to an improved wind retrieval. While this is generally true, comparing SCAT and WindRad, the increased number of WindRad views on their own provide a strong improvement in the outer swath, but it appears not effective in the sweet and nadir swath. The azimuths in the nadir swath are always either looking forward of the satellite track or looking backward. The increased views in this case will still be with similar azimuths, and these are not effective to improve the azimuth diversity. In the sweet swath, there are up to 18 views in the WVCs leading to a more diverse observation geometry.

One question is raised here: is the azimuth diversity the major influencer in the wind retrieval quality or the number of views with similar azimuth also give added value in the wind retrieval process? The views with similar azimuth geometry are averaged together into one super view. This influences most of the nadir swath since the views are with mainly forward and backward azimuths. Figure 23 shows that the views with similar azimuth angle in one of the nadir WVCs are aggregated into one view and the views for the nadir swath becomes mainly one forward and one backward. The wind retrieval results (Figure 24) in comparison with the normal wind retrieval results (Figure 17) show that the wind retrieval result with all the WVCs looks very similar, which seems that the views with similar azimuth angle do not have much added value onto the wind retrieval process, but when the outer swath WVCs are excluded from the result, wind speed and wind direction (Figure 24(b)) are both worse than Figure 17(b) as well as when excluding the nadir swath. In Figure 17(b) and (c), the nadir swath does not influence the wind speed retrieval much, while here (Figure 24(b) and (c)) the wind speed and wind direction

Deleted: Figure 16

Formatted: Font: (Default) Times New Roman, 10 pt, Not Bold, Font color: Auto, English (UK), Snap to grid

Deleted: Figure 17

Formatted: Font: (Default) Times New Roman, 10 pt, Not Bold, Font color: Auto, English (UK), Snap to grid

Formatted: Font: Times New Roman, Font color: Auto, English (UK), Snap to grid

Formatted: Font: Times New Roman, Font color: Auto, English (UK), Snap to grid

Formatted: Font: (Default) Times New Roman, 10 pt, Not Bold, Font color: Auto, English (UK), Snap to grid

Formatted: Font: Times New Roman, Font color: Auto, English (UK), Snap to grid

Formatted: Font: (Default) Times New Roman, 10 pt, Not Bold, Font color: Auto, English (UK), Snap to grid

Formatted: Font: (Default) Times New Roman, 10 pt, Not Bold, Font color: Auto, English (UK), Snap to grid

Formatted: Font: Times New Roman, Font color: Auto, English (UK), Snap to grid

retrieval results are obviously improved after excluding nadir swath. This means the reduction of the number of views in the nadir swath after aggregating the views with similar azimuth angle into one view leads to a worse wind retrieval quality.

The incidence angle range of SCAT, with almost 25 degrees, is much broader than that from WindRad at about 10 degrees, where, moreover, the minimum SCAT incidence angle at 25 degrees is about 10 degrees lower than that from WindRad. This implies that, while moving away from nadir, the azimuth diversity of SCAT increases much faster than that of WindRad, hence the steep performance increase for SCAT when moving away from nadir. On the other side, the many channels on WindRad and its fan beam add a lot of additional views and azimuth diversity near the outer swath, as compared to SCAT and SeaWinds, hence the outstanding outer swath performance of WindRad. We found that the number of slices located in the outer swath is the least and the geometrically unbalanced σ° distribution within the views of a WVC is one of reasons for the low retrieval quality. The instrument noise also contributes, and it is lower for WindRad than SCAT on average.

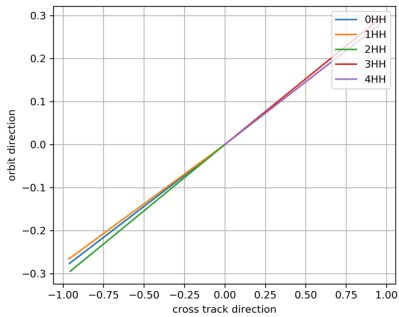
All in all, the wind retrieval is substantially better in the outer swath for WindRad. We also note that SCAT is essentially providing reference wind information for the CFOSAT small-incidence wave instrument SWIM and as such well designed for this task.

Deleted: However, the

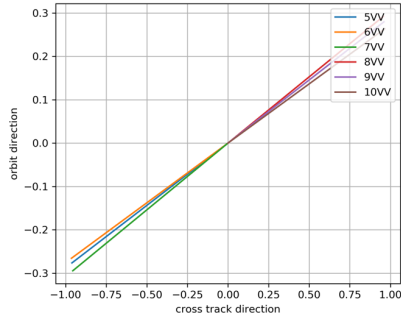
Formatted: Font color: Text 1

Deleted:

5



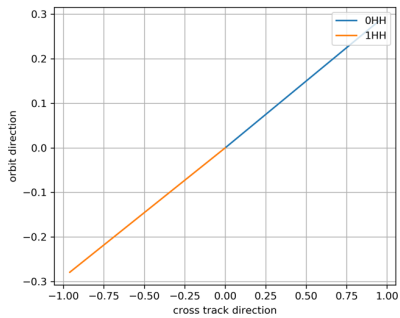
(a)



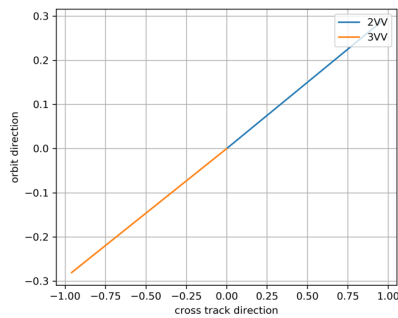
(b)

10

15



(c)



(d)

20

25

Figure 23: Azimuth angle distribution of the WVC located at the nadir swath (the values of x-axis and y-axis are for the angle display, they do not have actual meanings, x-axis is the cross track direction, y-axis is the satellite moving direction). (a) azimuth angles of the views with HH polarization. (b) azimuth angles of the views with VV polarization. (c) azimuth angles of the views with HH polarization (views with similar azimuth angles are aggregated into one view). (d) azimuth angles of the views with VV polarization (views with similar azimuth angles are aggregated into one view).

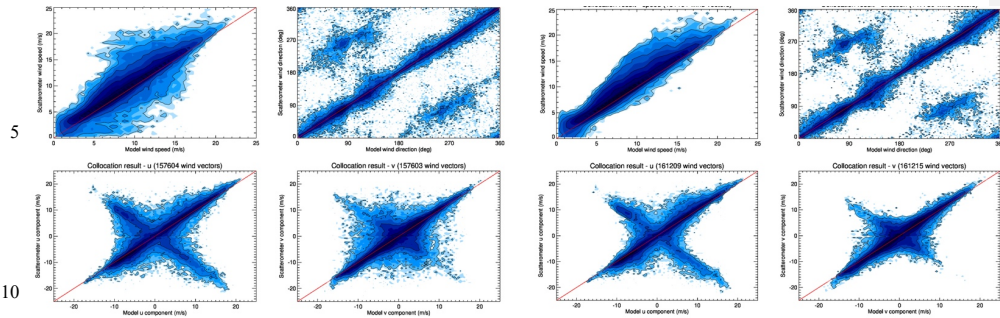
30

35

Formatted: Indent: First line: 0"

Formatted: Indent: First line: 0"

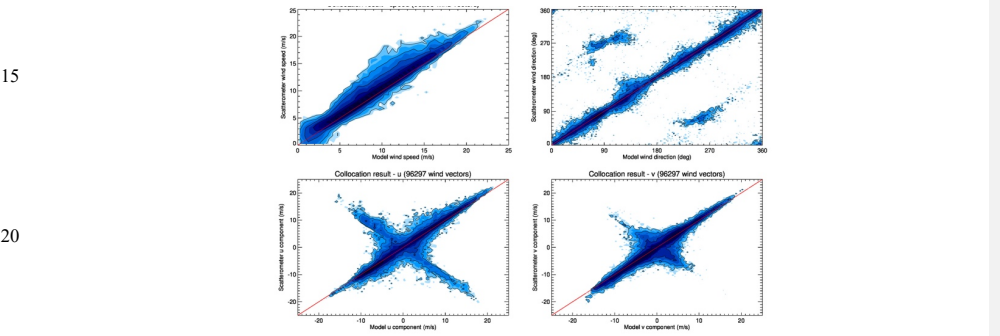
Formatted: Normal



(a)

(b)

Formatted: Font: Bold
Formatted: Font: Bold



(c)

Formatted: Font: 10 pt
Formatted: Font: 10 pt, Not Bold
Formatted: Font: 10 pt
Formatted: Font: 10 pt, Not Bold
Formatted: Font: (Default) +Body (Times New Roman), 9 pt, Bold, Font color: Text 1
Formatted: Caption, Indent: First line: 0", Line spacing: single

25 **Figure 24: Contoured histograms of SCAT retrieved 1st rank wind solution (aggregated the views with similar azimuth angle into one view) versus input wind field for 4 orbits. (a) all WVCs within the swath; (b) excluding the WVCs in the outer swath, WVC number from 8 to 42 are included; (c) excluding the WVCs in the outer swath and nadir swath, WVC number from 8 to 17 and 26 to 42 are included. From (a) to (c), upper left: wind speed; upper right: wind direction; lower left: u component; lower right: v component. The contour lines are logarithmic.**

5. Conclusions

In summary, we have presented and assessed a generic simulation framework, which has been adapted to all existing rotating-beam scatterometer types. The representative set of SCAT, WindRad and SeaWinds is chosen to evaluate the wind retrieval performance of the rotating scatterometers using Ku-band. The wind retrieval quality strongly depends on the location of the WVCs across the swath, and the sweet swath shows the most favorable geometries for wind retrieval. Among the more unfavorable outer and nadir swath regions, SCAT and SeaWinds both perform best in the nadir swath, while WindRad rather substantially improves the outer swath wind retrieval. On the other side, WindRad's nadir swath region with lower wind retrieval quality is larger than its outer swath region, while SCAT and SeaWinds have a relatively large outer swath region with degraded quality. The outer swath of SCAT implies both wind speed and wind direction retrieval problems, while for WindRad only wind speed retrieval is affected. Although rotating fan-beam scatterometers, particularly SCAT, much improve nadir performance with respect to SeaWinds. the nadir swath shows still significant wind direction ambiguity for both SCAT and WindRad.

The increased number of views in the nadir and sweet swath for WindRad does not lead to an improved wind retrieval, but it shows a saturation effect and stays relatively similar to SCAT. The retrieved wind direction has a tendency towards the satellite motion direction for all three instruments, which is related to the retrieval procedure. Rain effect is not taken into consideration, so the rain disturbance in Ku-band and the advantage of the C-band on WindRad cannot be shown here. Further studies may focus on this aspect.

To facilitate good quality collocations with the CFOSAT SWIM instrument, the SCAT design is clearly focused on an optimal performance close to nadir and employs small incidence angles, combined with a large incidence angle range. This facilitates the availability of additional views near nadir with enhanced azimuth and incidence angle diversity. On the other hand, WindRad's most useful complement is clearly its dual frequency capability, providing many views in the outer swath, where excellent performance is obtained according to our simulations.

This simulation allows us to further investigate the true resolution of the instruments before their launch and also the non-overlap of the views in a WVC, which contributes to the geophysical noise. The WVC size is not the true spatial resolution and neither the true representation of the contributing views, which depend on the spatial response function of each sample, how these are aggregated into a view and which views contribute to the WVC (Vogelzang et al., 2017; Vogelzang and Stoffelen, 2017). For rotating-beam scatterometers the sampling and hence wind retrieval characteristics vary potentially both by across-track and along-track WVC, which may be further investigated. Such development may much help users interested in coastal winds.

Our simulation does not consider the rain effect. Ku-band ocean returns are affected by rain, and moderate and heavy rain will certainly degrade the wind retrieval. At KNMI, we use the wind retrieval MLE for rain screening of Ku-band systems, much aided by MSS 2DVAR. This successful methodology developed for SeaWinds will also be attempted for

CFOSAT. On the other hand, C-band backscatter is much less sensitive to rain and included in WindRad. This advantage of WindRad should be further investigated, e.g., by using collocated measurements of Ku-band and C-band scatterometers.

The broad user community looks forward to an increased temporal sampling of the ocean surface with scatterometer winds, such as with both WindRad and SCAT, that will be useful contributions to the global ocean surface vector winds

5 virtual constellation.

Acknowledgments: This work was supported by the project of 'the development and provision of scatterometer wind processing software and wind products for the China-France Oceanography SATellite (CFOSAT)' between CNES (Centre National d'etudes Spatiales) and KNMI (Royal Netherlands Meteorological Institute), supported by the EUMETSAT Ocean and Sea Ice Satellite Application Facility (OSI SAF).

10

References

Bajo, M., De Biasio, F., Umgiesser, G., Vignudelli, S. and Zecchetto, S.: Impact of using scatterometer and altimeter data on storm surge forecasting, *Ocean Model.*, 113, 85–94, doi:10.1016/j.ocemod.2017.03.014, 2017.

Chi, C. Y. and Li, F. K.: A comparative study of several wind estimation algorithms for spaceborne scatterometers, *IEEE*
15 *Trans. Geosci. Remote Sens.*, 26(2), 115–121, doi:10.1109/36.3011, 1988.

Dou, F., Yin, H. and Gu, S.: Simulation of wind performance in tropical cyclone for China's future dual-frequency wind field radar, in *Proc. of SPIE*, vol. 9264, pp. 92641G1-92641G7., 2014.

Dunbar, R. S., Hsiao, S. V., Kim, Y., Pak, K. S., Weiss, B. H. and Zhang, A.: *Science Algorithm Specification*, Jet Propuls., 2001.

20 Gelsthorpe, R. V., Schied, E. and Wilson, J. J. W.: *ASCAT - Metop's advanced scatterometer*, ESA Bull. Sp. AGENCY, 2000.

Hoffman, R. N. and Leidner, S. M.: *An Introduction to the Near – Real – Time QuikSCAT Data*, *Weather Forecast.*, 20, 476–493, 2005.

Hoots, F. R. and Roehrich, R. L.: *Spacetrack Report No. 3-Models for Propagation of NORAD Elements Sets.*, 1980.

25 Jiang, X., Lin, M., Liu, J., Zhang, Y., Xie, X., Peng, H. and Zhou, W.: The HY-2 satellite and its preliminary assessment, *Int. J. Digit. Earth*, doi:10.1080/17538947.2012.658685, 2012.

JPL: *QuikSCAT Science Data Product User's Manual.*, 2001.

Li, Z., Verhoef, A. and Stofflen, A.: *CWDP L1B simulator and L2A processor Specification and User Manual*, de Bilt, the Netherlands., 2017.

30 Lin, C.-C., Rommen, B., Wilson, J. J. W., Impagnatiello, F. and Park, P. S.: An analysis of a rotating, range-gated, fanbeam spaceborne scatterometer concept, *Geosci. Remote Sensing*, *IEEE Trans.*, doi:10.1109/36.868870, 2000a.

- Lin, C.-C., Stoffelen, A., De Kloe, J., Wismann, V., Bartha, S. and Schulte, H.-R.: Wind retrieval capability of rotating, range-gated, fanbeam spaceborne scatterometer, in Proc. SPIE Int. Symp. Remote Sens., pp. 268–285, Crete, Greece., 2002.
- Lin, C. C., Rommen, B., Wilson, J. J. W., Impagnatiello, F. and Park, P. S.: An analysis of a rotating, range-gated, fanbeam spaceborne scatterometer concept, IEEE Trans. Geosci. Remote Sens., 35(5), 2114–2121, doi:10.1109/36.868870, 2000b.
- 5 Lin, W. and Dong, X.: Design and optimization of a Ku-band rotating, range-gated fanbeam scatterometer, Int. J. Remote Sens., 32(8), 2151–2171, doi:10.1080/01431161003674626, 2011.
- Liu, W. T., Tang, W. and Xie, X.: wind power distribution over the ocean, Geophys. Res. Lett., 35(L13808), 1–6, 2008.
- Long, D. G., Yoho, P. K., Yoho, P. K., Long, D. G. and Member, S.: Correlation and covariance of satellite scatterometer measurements, IEEE Trans. Geosci. Remote Sens., 42(6), 1179–1187, 2004.
- 10 Naderi, F. M., Freilich, M. H. and Long, D. G.: Spaceborne Radar Measurement of Wind Velocity Over the Ocean—An Overview of the NSCAT Scatterometer System, Proc. IEEE, doi:10.1109/5.90163, 1991.
- Offiler, D.: A comparison of SEASAT scatterometer-derived winds with JASIN surface winds, Int. J. Remote Sens., doi:10.1080/01431168408948814, 1984.
- Pierson, W. J.: Probabilities and statistics for backscatter estimates obtained by a scatterometer, J. Geophys. Res., 94(C7),
 15 9743–9759, doi:10.1029/JC094iC07p09743, 1989.
- Portabella, M.: Wind Field Retrieval from Satellite Radar Systems., 2002.
- Portabella, M. and Stoffelen, A.: Characterization of residual information for SeaWinds quality control, IEEE Trans. Geosci. Remote Sens., doi:10.1109/TGRS.2002.807750, 2002.
- Rivas, M. B., De Kloe, J. and Stoffelen, A.: Study of an Objective Performance Measure for Spaceborne Wind Sensors, de
 20 Bilt, the Netherlands., 2009.
- Singh, R., Kumar, P. and Pal, P. K.: Assimilation of oceansat-2-scatterometer-derived surface winds in the weather research and forecasting model, IEEE Trans. Geosci. Remote Sens., doi:10.1109/TGRS.2011.2164410, 2012.
- Stoffelen, A. and Anderson, D.: Ambiguity removal and assimilation of scatterometer data, , 123, 491–518, 1997.
- Stoffelen, A. and Portabella, M.: On Bayesian Scatterometer Wind Inversion, IEEE Trans. Geosci. Remote Sens., 44(6), 1–
 25 11, doi:10.1109/TGRS.2005.862502, 2006.
- Ulaby, F. and Long, D. G.: Microwave Radar and Radiometric Remote Sensing, edited by A. Arbor, University of Michigan Press, Michigan., 2013.
- Vogelzang, J.: Two-dimensional variational ambiguity removal (2DVAR), de Bilt, the Netherlands., 2013.

Vogelzang, J. and Stoffelen, A.: ASCAT Ultrahigh-Resolution Wind Products on Optimized Grids, *IEEE J. Sel. Top. Appl. EARTH Obs. Remote Sens.*, 10(5), 2332–2339, 2017.

Vogelzang, J., Verhoef, A., De Vries, J. and Bonekamp, H.: Validation of Two-Dimensional Variational Ambiguity Removal on SeaWinds Scatterometer Data, *J. Atmos. Ocean. Technol.*, 26, 1229–1245, doi:10.1175/2008JTECHA1232.1, 5 2009.

Vogelzang, J., Stoffelen, A., Lindsley, R. D., Verhoef, A. and Verspeek, J.: The ASCAT 6.25-km wind product, *IEEE J. Sel. Top. Appl. EARTH Obs. Remote Sens.*, 10(5), 2321–2331, 2017.

de Vries, J., Stoffelen, A. and Beysens, J.: Ambiguity Removal and Product Monitoring for SeaWinds, de Bilt, the Netherlands. [online] Available from: <http://www.knmi.nl/scatterometer/publications/>, 2005.

10 Wang, Z., Stoffelen, A., He, Y., Zhang, B., Verhoef, A., Lin, W., Li, X. and Shao, F.: An improved wind direction modulation for Ku-band geophysical model functions , based on ASCAT and SCATSAT-1 collocations Key Points, n.d.

